NACA RM E53H04

NACA

RESEARCH MEMORANDUM

INVESTIGATION AT MACH NUMBERS 1.5 AND 1.7 OF TWIN-DUCT SIDE AIR-INTAKE SYSTEM WITH 9° COMPRESSION RAMP INCLUDING MODIFICATIONS TO BOUNDARY-LAYER-REMOVAL WEDGES AND EFFECTS OF A BYPASS SYSTEM

By Leonard J. Obery and Leonard E. Stitt

Lewis Flight Propulsion Laboratory
Cleveland, Ohio

NATIONAL ADVISORY COMMITTEE
FOR AERONAUTICS

WASHINGTON

October 12, 1953
Declassified October 16, 1961

NATIONAL ADVISORY COMMITTEE FOR AERONAUTICS

RESEARCH MEMORANDUM

INVESTIGATION AT MACH NUMBERS 1.5 AND 1.7 OF TWIN-DUCT SIDE AIR-INTAKE SYSTEM WITH 9° COMPRESSION RAMP INCLUDING MODIFICATIONS TO BOUNDARY-LAYER-REMOVAL WEDGES AND EFFECTS OF A BYPASS SYSTEM

By Leonard J. Obery and Leonard E. Stitt

SUMMARY

The performance of a twin-duct air-intake system with a 9° compression-ramp inlet mounted on a supersonic airplane was investigated in the Lewis 8- by 6-foot supersonic wind tunnel at free-stream Mach numbers of 1.5 and 1.7 over a range of angles of attack, yaw, and mass-flow ratios. The effect on over-all performance of a series of boundary-layer-removal wedges and a main-duct air-flow bypass system were also investigated. Higher pressure recoveries were obtained with the configuration having a 9° compression-ramp inlet than with a similar configuration in a previous investigation with a 6° ramp inlet. The 9° ramp eliminated ramp boundary-layer separation and resulted in higher total-pressure recovery at a Mach number of 1.5, while at 1.7 the reduced region of separation and the reduced supersonic loss attendant with the higher ramp angle caused the increased total-pressure recovery. At lowered mass-flow ratios for a free-stream Mach number of 1.5, symmetrical total-pressure-recovery contours at the diffuser exit resulted from the elimination of ramp separation. At Mach number 1.7 for the 9° inlet and at Mach numbers of 1.5 and 1.7 for the 6° inlet, ramp separation caused asymmetrical contours at the diffuser exit. At very low mass flows, the twin-duct system operated with stable inlet shocks; however, one duct operated supercritically, whereas the other duct carried little or no mass flow.

Modifications to the boundary-layer-removal system indicated that, for this configuration, the deflection angle and the longitudinal location of the wedges had little effect on inlet performance provided the bleed duct remained open, whereas deflection of all the boundary-layer air by wedges considerably reduced inlet performance. Results of the bypass investigation indicated that reduced engine mass flows could be obtained with only a small increase in external drag and that satisfactory operation could be expected with a cowl-flap-type door opening into the air stream.

INTRODUCTION

An investigation was conducted in the 8- by 6-foot supersonic tunnel of the NACA Lewis laboratory to evaluate the internal and external performance of a twin-duct air-intake system mounted on a supersonic airplane. The results of the part of this investigation using a 6° compression-ramp inlet with various inlet modifications were reported in reference 1. The present report discusses (1) the results obtained with a 9° compression-ramp inlet, (2) the effects on performance of modifications to the boundary-layer-removal system, and (3) the performance of a particular bypass system. An efficiency comparison of several of the air-induction configurations is made based on the J57-P-7 engine.

The investigation was conducted over a range of angles of attack and yaw at free-stream Mach numbers of 1.5 and 1.7. The Reynolds number of the test, based on the length of fuselage ahead of the inlet, was approximately 14×10^6.

SYMBOLS

The following symbols are used in this report:

A	area
C_D	external drag coefficient based on maximum frontal cross-sectional area of 2.097 sq ft, $D/q_0 A_f$
$C_{T,B}$	boundary-layer bleed duct thrust coefficient based on maximum frontal cross-sectional area of 2.097 sq ft
C_{T-D}	coefficient of internal thrust minus external drag based on maximum frontal cross-sectional area of 2.097 sq ft
D	drag
F_n	engine thrust at diffuser total-pressure recovery
$F_{n,id}$	engine thrust at 100-percent diffuser total-pressure recovery
L	length of subsonic diffuser, 74 in.
M	Mach number
m_B/m_0	boundary-layer bleed duct mass-flow ratio, $\frac{\text{boundary-layer mass flow}}{\rho_0 V_0 A_{i,B}}$

m_b/m_0 bypass mass-flow ratio, $\frac{\text{bypass mass flow}}{\rho_0 V_0 A_i}$

m_3/m_0 engine mass-flow ratio, $\frac{\text{engine mass flow}}{\rho_0 V_0 A_i}$

P total pressure

p static pressure

q dynamic pressure, $\gamma p M^2/2$

V velocity

X distance from cowl lip, model station 36

α model angle of attack with respect to main fuselage axis, deg

γ ratio of specific heats, 1.40

ρ mass density of air

Subscripts:

B boundary-layer bleed duct-exit survey station, model station 101.105

b bypass

c mass-flow static-pressure station

f frontal

i inlet

X conditions at X-distance from cowl lip

0 free steam

1 fuselage survey station, model station 31

2 diffuser-inlet survey station, model station 37.50

3 diffuser-exit survey station, model station 102.105

Pertinent areas:

A_f maximum frontal cross-sectional area, 2.097 sq ft

A_i inlet capture area of both ducts defined by cowl lip (and ramp leading edge), 0.256 sq ft

$A_{i,B}$ inlet area of one boundary-layer bleed duct, 0.00862 sq ft

A_3 flow area at diffuser discharge, 0.326 sq ft

APPARATUS AND PROCEDURE

As shown photographically in figure 1 and schematically in figure 2, the model of the present test was a quarter-scale fuselage forebody of a supersonic aircraft. Twin-scoop ramp-type inlets were located on the fuselage sides, with the ducts joining in a common annular passage near the aft end of the model. In the prototype airplane this station would correspond to the engine compressor face.

The model was sting-supported and connected to the sting through an internal strain-gage balance. A shroud, used to protect various mechanisms, was attached to the sting but was entirely independent of the model. As can be seen in figure 1, the shroud formed a continuation of the aft fuselage. The reverse scoops near the top of the shroud were used to lower the pressure inside the shroud to insure choking at the plugs.

The forward section of the airplane, including the inlet, was canted 5° downward with respect to the main fuselage axis as shown in figure 2. The downward cant was utilized to facilitate pilot vision in the prototype rather than to provide maximum performance of the inlet at the cruise angle of attack. Also shown in figure 2 are the internal air-flow stations and the main-duct and boundary-layer-duct plugs used to control the respective mass flows.

A photograph of one of the inlets showing the cowl shape is presented in figure 3. The 9° compression-ramp leading edge was longitudinally located to cause the resulting oblique shock wave to intersect the outer cowl lip at a free-stream Mach number of approximately 1.75. The side view of the inlet, shown in figure 4(b), indicates the reverse curvature of the external fairing on the top and bottom of the inlet. This curvature resulted from sharpening the cowl leading edges and faired out until a smooth fairing resulted at the cowl lip (fig. 4(c)). The twin inlets had geometrically similar internal subsonic diffuser ducts which changed smoothly from a nearly rectangular form at the entrance (model station 36) to an annular cross section at the junction of the two ducts (model station 101). Typical duct cross sections and the resulting area variation are presented in figure 5. The longitudinal area variation of the subsonic diffuser is presented as the ratio of the local flow area to the maximum flow area at the diffuser discharge.

Ram-type boundary-layer scoops were located beneath the center portion of the inlet ramp for removal of the fuselage boundary-layer air. Internal boundary-layer ducts continued aft of the scoops and made a transition from a rectangular cross section at the entrance to a circular cross section at the exit. The bleed ducts discharged parallel to the main air-flow duct at the exit station. The boundary-layer air in excess of that passing through the bleed ducts was spilled around the open-scoop sides by boundary-layer wedges as shown in figures 2 and 3. The boundary-layer scoop height was fixed at 0.30 inch to correspond to the experimentally determined fuselage boundary-layer thickness at the inlet station for free-stream Mach numbers of 1.5 and 1.7 (ref. 1).

Variations of the boundary-layer wedges are shown photographically in figure 6 and in detail in figure 7. The boundary-layer wedge modifications varied the longitudinal location of the wedge vertices and also the discharge angle of the open-scoop sides. As seen in figure 7(a), the first series of modifications to the boundary-layer wedges consisted of closing the boundary-layer duct and forming 50° half-angle wedges to deflect the boundary-layer air. The vertex of the first 50° wedge was longitudinally located 1 inch back from the ramp leading edge and is designated by a code as 50-1-C. The first number refers to the wedge half-angle, the second to the distance in inches aft of the ramp leading edge, and the letter C refers to the closed bleed duct. The second series of modifications formed 30°, 40°, and 50° half-angle wedges 1 inch aft of the ramp leading edge (fig. 7(b)). In this series the bleed duct remained open, as designated in the code by the letter O as the third symbol.

As a further modification of the 9° inlet configuration, a variable-area main-duct bypass system, shown photographically in figure 8 and in detail in figure 9, was located at model station 70 with one such bypass provided for each main duct. The bypass, essentially a convergent nozzle, was capable of discharging up to 30 percent of the maximum mass flow captured by the inlet. Remote actuation of the bypass door was accomplished by driving the gear sector forming the side trailing edges as shown in figure 8. This particular bypass was designed to be a simple mechanical system readily adaptable to a production aircraft in order to determine whether a compromised system could satisfactorily maintain the advantages inherent in a more idealized bypass system, such as that discussed in reference 2. The bypass door, for example, opened into the air stream in the manner of nacelle cowl flaps, thereby creating additional body drag and also causing the bypassed air to discharge away from an axial direction.

The instrumentation for this model was similar to that reported in reference 1. Body angle of attack was measured with an internal angle-of-attack indicator, and flow stability was measured with pressure-sensitive pickups. As in reference 1, the force-measuring system

consisted of an internal strain-gage balance, located at a forward model station, and a strain-gage link mounted between the sting and the rear model bulkhead. The rear link was mounted so as to measure only a normal force component without influencing the axial force and, additionally, to restrain the model in pitch, thereby eliminating most of the model deflection due to imposed air loads.

During the conduct of the tests, the boundary-layer bleed plug was held at a particular area ratio, so that the internal force developed by the boundary-layer bleed duct would be approximately constant for all configurations. In general, with the bypass system in operation, a constant main-duct exit Mach number was set and the bypass doors were opened, thus discharging progressively more flow, while, because of the relieved back pressure, the inlet captured a correspondingly increased flow. The bypass-area ratio was also set at particular values for each exit Mach number, so that an extrapolation to conditions of fixed bypass at various main-duct exit Mach numbers could also be made.

The mass flow through the main duct was computed from a measured static pressure at station c, with the assumption that the flow was choked at the area determined by the mass-flow control plug, and is believed accurate within ± 2 percent. The main-duct mass-flow ratio is the ratio of the mass flowing through the ducts to that flowing in the free stream through an area equal to the projected inlet area of both ducts. The total-pressure recovery at station 3 was determined from the static pressure at station 3 and from the calculated mass flow to an accuracy better than ± 1 percent. For one phase of the test, the boundary-layer bleed performance was investigated through a mass-flow range, and the resulting mass-flow ratios were calculated from static- and total-pressure measurements at the bleed exit. From the consistency of the data, these values are believed accurate to ± 3 percent and the measured total-pressure recoveries to ± 1 percent. The boundary-layer bleed mass-flow ratios are based on the bleed-inlet area as the reference area.

The bypass mass-flow ratios were computed from the sonic discharge area, assumed to be the minimum geometric area for all openings of the bypass, and from the total-pressure recovery in the main duct. Bypass mass-flow ratios were corrected for an effective discharge area and total pressure at supercritical inlet flow by evaluating bypass mass-flow ratio as the difference between engine mass-flow ratios with and without bypass; this correction factor, assumed constant for computation of the bypass mass flows for subcritical inlet flow, was of the order of 0.99. The bypass mass-flow ratios and total-pressure recoveries are believed accurate to the same order as the corresponding main-duct quantities.

In this report drag is defined as the streamwise component of the external forces, not including the base pressure force or the stream thrust developed by the main-duct flow from free stream to exit. The drag, however, does include the force developed by the internal flow through the boundary-layer bleed ducts and the bypass system when in operation. The boundary-layer force was calculated for the range of boundary-layer bleed mass-flow ratios as the change in total momentum from the bleed inlet to the bleed exit.

The Reynolds number based on the length of the fuselage ahead of the inlets varied from 13×10^6 to 15×10^6 at a Mach number of 1.5 and from 13×10^6 to 16×10^6 at a Mach number of 1.7.

RESULTS AND DISCUSSION

The internal performance and the forebody drag of the configuration are presented in figure 10. The total-pressure-recovery curves for a free-stream Mach number of 1.5 indicate an increased recovery with decreasing mass-flow ratio throughout most of the subcritical region at all angles of attack, as contrasted to a constant or reduced recovery for M_0 of 1.7. For both values of M_0, however, the highest internal performance occurred at an angle of attack of 5°, since at that angle of attack the inlet was alined with the flow because of the droop of the forward section. As a result of this characteristic, detailed comparisons and representative data are shown at a body angle of attack of 5°, while data at an angle of attack of 1.5° are presented to show the performance at the prototype supersonic cruise angle of attack. The critical and peak total-pressure recoveries of this inlet were as great as, or greater than, any of the total-pressure recoveries of the 6° inlets of reference 1 at all corresponding angles of attack. As will be shown later, the higher recoveries at M_0 of 1.5 resulted from the elimination of flow separation on the ramp, while at M_0 of 1.7 the increased performance resulted from a reduction in the size of the separated region and from the lower inlet shock losses attendant with a 9° ramp.

The maximum mass-flow ratio attained with the 9° ramp inlet at an angle of attack of 5° was approximately $3\frac{1}{2}$ percent less than theoretical at M_0 of 1.5 and $5\frac{1}{2}$ percent less at M_0 of 1.7, probably because of a combination of total-pressure loss ahead of the inlet and the existence of a curved shock from the ramp in place of the theoretical straight-line shock. Operation of the twin-duct system at very low mass-flow ratios resulted in a stable inlet shock pattern; however, one duct operated supercritically, whereas the other duct carried little or no mass flow.

The minimum drag coefficient of the body was considerably greater than that of the aircraft forebody reported in reference 3. The high drag probably resulted from the bluntness of the drooped nose and the large projected area caused by the external fairing of the twin ducts. The forebody drag rise was approximately the same at M_0 of 1.5 and 1.7 and was about half the magnitude obtained from similar investigations or predicted by various theories. Because of the pressure drag on the reverse curvature of the inlet cowl lips, the minimum drag was higher than that reported in reference 1.

Contours of total-pressure recovery at the inlet (station 2) are presented in figure 11 for M_0 of 1.5 and 1.7 and angles of attack of 5° and 1.5°. At M_0 of 1.5 for high subcritical and supercritical flow (fig. 11(a)), the recovery was reasonably constant at a high value over the face of the inlet except at the duct corners. Reducing the mass flow at an angle of attack of 5° (fig. 11(b)) caused a thickening of the ramp boundary layer and also reduced the pressure recovery near the ceiling half of the inlet, possibly because of the increased turning losses occasioned by the 9° ramp with the cowl designed for flow from a 6° ramp. At an angle of attack of 1.5° near critical flow (fig. 11(c)), the contours again indicate a generally uniform flow, with a high-pressure region located near the ramp half of the inlet. At M_0 of 1.7, as contrasted to M_0 of 1.5, the higher losses generally occurred near the ramp. Regions of separated flow are evidenced at the near critical condition (fig. 11(d)), while at the lower mass-flow ratio (fig. 11(e)) reverse flow occurred on the ramp near the bottom corner. At an angle of attack of 1.5° (fig. 11(f)), the region of reverse flow shifted to the top corner, probably because that is the leeward side of the cowl lip, and separated flow is again evidenced.

The total-pressure contours at station 3 for M_0 of 1.5 and angles of attack of 5° and 1.5° (figs. 12(a) to 12(c)) indicate approximately equal flow through both ducts from their symmetrical appearance throughout the range of mass-flow ratios. However, at M_0 of 1.7 (figs. 12(d) to 12(f)), apparently one duct is taking most of the flow, particularly at the lower mass-flow ratio. The asymmetrical flow shown at M_0 of 1.7 (fig. 12(e)) probably results from ramp separation, since symmetrical contours were obtained at M_0 of 1.5 (fig. 12(b)), where no separation occurred. This presumption is further justified by a comparison with the 6° ramp data of reference 1. Ramp separation occurred with the 6° inlet at M_0 of 1.5, and asymmetrical contours were obtained, especially at the lower mass-flow ratios. When the separation was eliminated with the 9° ramp, symmetrical flow resulted.

The breakdown of total-pressure ratio losses, as presented in figure 13, indicates approximately the same loss ahead of the inlet for both M_0 of 1.5 and 1.7 at an angle of attack of 5°. The estimated values of subsonic losses shown in figure 13 were calculated using an adaptation of the method of reference 4. At critical mass-flow ratio, the curves indicate that for M_0 of 1.5 the subsonic losses $\Delta P_{2-3}/P_0$ represented a considerable part of the over-all losses, while at M_0 of 1.7 the supersonic losses $\Delta P_{1-2}/P_0$ accounted for the larger part of the losses. At M_0 of 1.5 the experimental supersonic losses were only about 1 percent greater than the estimated values. As shown by the contours of inlet total-pressure recovery for M_0 of 1.5 at critical flow (fig. 11(a)), the theoretical values of pressure recovery were attained except at the corner of the duct. It is expected that these regions accounted for the 1-percent difference between estimated and experimental supersonic recovery. For critical flow at M_0 of 1.7, the experimental supersonic losses were over $2\frac{1}{2}$ percent greater than the estimated value. The inlet contours (fig. 11(d)) show that the theoretical recovery was attained over part of the inlet, but they also indicate a very thick boundary layer with the probability of separated flow near the ramp surface, accounting for the difference between experimental and estimated supersonic recovery. In the subcritical region for M_0 of 1.5, the increased supersonic loss occurred as a result of thickening of the ramp boundary layer and reduced recovery near the outer cowl lip; at M_0 of 1.7, the increased subcritical losses resulted from the thick ramp boundary layer and separated flow at the ramp surface, as indicated by the inlet contours (fig. 11).

Schlieren photographs of the inlet at various conditions (fig. 14) show the flow separating from the ramp at M_0 of 1.7, but not at M_0 of 1.5. These photographs were taken with the model at a zero angle of yaw, corresponding to an inlet angle of attack of about -5° as a result of the droop of the forward section. However, it is believed that similar flow would be attained at an inlet angle of attack of zero degrees.

The internal performance of the configuration over a range of angles of yaw and mass-flow ratios is presented in figure 15 for M_0 of 1.5. The performance throughout the yaw range was obtained with the body at zero degrees angle of attack and, consequently, with an inlet angle of attack of -5°. No performance data were obtained for the yaw conditions at M_0 of 1.7. Figure 15 indicates only slight reductions in critical-pressure recovery and critical mass-flow ratio throughout the yaw range investigated. Diffuser-exit total-pressure-recovery contours are presented in figure 16 for high and low values

of mass-flow ratio for angles of yaw of 3° and 6° at M_0 of 1.5. Total-pressure contours for an angle of yaw of zero (not included in fig. 16) indicate symmetrical flow through both ducts at high and low values of mass-flow ratio. For angles of yaw greater than zero, the total-pressure contours indicate more mass flow through the windward duct and higher total-pressure recovery in the corresponding half of the diffuser-exit station than obtained in the leeward duct. These conditions become more pronounced as the yaw angle increases.

The internal performance of one of the boundary-layer bleed ducts is presented in figure 17 for an angle of attack of 5° at M_0 of 1.5 and 1.7. At M_0 of 1.5, the bleed attained a higher supercritical mass-flow ratio and also a higher pressure recovery over the entire flow range than at M_0 of 1.7. The thrust-force coefficient of the bleed duct is defined herein as the change in momentum from the bleed inlet to the bleed exit. Thus the thrust-force coefficient does not include the drag associated with the skin friction over the forward part of the body washed by the bleed mass flow, nor does it include the additive thrust term usually associated with duct flow requiring the addition of the additive drag component. The thrust force, developed in the model by the action of the boundary-layer bleed plug, was inherent to the manner of testing, since, of course, in an actual installation the boundary-layer bleed duct without heat addition would produce only drag. The forebody drag coefficient of the configuration includes this bleed-thrust force. However, for all the data presented, the bleed Mach number ahead of the plug M_B was held at 0.254 for M_0 of 1.5 and at 0.275 for M_0 of 1.7, where the internal force developed by the bleed system was approximately zero as shown in figure 17. Furthermore, at all operating conditions of the bleed duct, this force was quite small; for example, at the lowest bleed Mach numbers M_B investigated, the internal force coefficient developed by both ducts was only about 0.006, which is almost within the accuracy of the present drag measurements.

To qualitatively establish the limits within which the boundary-layer-removal system could be varied without affecting over-all performance, several modifications to the system were made. Figures 18 and 19 show the effect on over-all performance of deflecting the boundary-layer air with high-angle wedges. With the vertex of the wedge 1 inch aft of the ramp leading edge, little or no change occurred in forebody drag, as seen from a comparison of figure 18 for the 50-1-C configuration with figure 10 for the unmodified configuration. However, the effect on internal performance of the 50-1-C configuration as compared with that of the unmodified configuration was quite pronounced. Lower supercritical mass-flow ratio, lower critical pressure recovery, and an immediate drop-off in pressure recovery in the subcritical range

resulted because of the distortion of the flow field ahead of the ramp. Moving the wedge vertices aft caused similar, but less pronounced, effects on internal performance, as shown in figure 19 for the 50-2.9-C configuration; again, within the accuracy of the measurements, the forebody drag remained unchanged. The effects noted on internal performance resulted directly from the blockage of the boundary-layer bleed duct, because the remaining boundary-layer wedge configurations (50-1-0, 40-1-0, 30-1-0) with the boundary-layer duct open had no effect on either internal performance or forebody drag. From the results of this investigation then, it may concluded that the angle of the wedge had a relatively small effect (50-1-0 compared with the unmodified configuration), while the amount of boundary-layer air pushed aside by the wedge was a determining factor on inlet performance (50-1-0 compared with 50-1-C).

The performance of a particular bypass system was investigated to determine whether this type system could provide reduced engine mass flow without incurring the usually high subcritical drags associated with normal shock spillage. In the following discussion, the engine mass-flow ratio is defined as the inlet mass-flow ratio minus the bypass mass-flow ratio. The internal performance of the configuration is presented in figure 20 over a range of engine mass-flow ratios for several constant openings of the bypass doors at M_0 of 1.7 and at angles of attack of 1.5° and 5°. Lines of constant M_3 are also indicated for the range of mass-flow ratios covered. The curves of constant bypass settings indicate that any engine mass-flow ratio within the usable range can be attained with critical inlet operation by spilling the mass flow through the bypass instead of behind the normal shock.

The variation of the coefficient of internal thrust minus forebody drag with bypass mass-flow ratio is presented in figure 21 for various values of M_3. It can be seen that, at a constant M_3, the thrust-minus-drag coefficient increases with increasing bypass mass-flow ratio until the inlet is operating at critical mass-flow ratio. Further increases in bypass mass-flow ratio result in a rapid decrease in thrust-minus-drag coefficient because of the reduction in total-pressure recovery associated with supercritical inlet operation.

The drag rise associated with reduced engine mass-flow ratios for the bypass configuration (fig. 22) was determined with optimum bypass settings corresponding to critical inlet flow at all engine mass-flow ratios. The drag rise of the configuration with bypass at optimum setting was approximately 1/3 of that obtained from experimental results with the configuration of reference 3 or expected from various theories. Compared with the no-bypass configuration of this report, only a small reduction in drag resulted because of the low drag rise of the no-bypass configuration mentioned earlier in the text. Thus, while the bypass

shows rather small gains with this particular installation, other configurations with a more usual drag rise might use this type of variable geometry advantageously.

Figure 23 presents the variation of engine efficiency parameter with M_3 for several configurations at M_0 of 1.7 and an angle of attack of 1.5°. This efficiency parameter is calculated for the configurations by utilizing the ideal thrust $F_{n,id}$ of the J57-P-7 engine at an altitude of 35,000 feet. The expression $F_n/F_{n,id}$ is the ratio of actual to ideal thrust resulting from the loss in total-pressure recovery, and ΔD is the increment of drag rise from minimum forebody drag. Values of engine efficiency at M_3 greater than 0.331 (engine match point for the present particular geometry) correspond to the efficiencies that would be obtained in the hypothetical case of reducing the inlet and ducting size while holding a constant engine-compressor area and assuming no total-pressure loss in the added expansion of the required transition section from the hypothetical station 3 to the engine area.

For the present configuration, figure 23 indicates that the reduced mass flow required to match the J57-P-7 engine could be obtained with an increase of 3 percent of the ideal thrust (or about 350 pounds of thrust) by using the bypass system. This gain in efficiency could be increased to 4 percent by eliminating the drag of the bypass doors that extended into the air stream and would correspond to an idealized bypass system. A considerably greater increase, perhaps of the order of $7\frac{1}{2}$ percent, would be expected had the subcritical drag rise of the configuration been nearer the estimated value.

SUMMARY OF RESULTS

An investigation was conducted in the 8- by 6-foot supersonic wind tunnel to determine the performance of a twin-duct air-intake system with a 9° compression-ramp mounted on a supersonic airplane at Mach numbers of 1.5 and 1.7. A previous investigation presented the performance of this air-intake system with a 6° compression ramp. In addition, modified boundary-layer-removal wedges and a main-duct bypass system were investigated. The following results were obtained:

1. The 9° ramp eliminated ramp boundary-layer separation at a Mach number of 1.5 and resulted in symmetrical flow at the diffuser exit at low mass-flow ratios as compared with asymmetrical flow with the 6° ramp. Asymmetrical flow was obtained at low mass-flow ratios at a Mach number of 1.7 as a result of ramp flow separation.

2. Higher pressure recoveries were obtained at a Mach number of 1.5 with the 9° ramp than with the 6° ramp because of the elimination of ramp flow separation; higher pressure recoveries were obtained at a Mach number of 1.7 with the 9° ramp than with the 6° ramp because of the reduction in the size of the separated region and the lower inlet shock losses attendant with the 9° ramp.

3. The internal performance of the inlet was affected by the design of the boundary-layer-removal system. For this configuration the amount of boundary-layer air deflected, rather than the deflection angle, was the determining factor on inlet performance.

4. The bypass system allowed reduced engine mass-flow ratios with a relatively small increase in external drag.

Lewis Flight Propulsion Laboratory
National Advisory Committee for Aeronautics
Cleveland, Ohio, August 6, 1953

REFERENCES

1. Davids, Joseph, and Wise, George A.: Investigation at Mach Numbers 1.5 and 1.7 of Twin-Duct Side Intake System with Two-Dimensional 6° Compression Ramps Mounted on a Supersonic Airplane. NACA RM E53H19, 1953.

2. Allen, J. L., and Beke, Andrew: Force and Pressure Recovery Characteristics at Supersonic Speeds of a Conical Spike Inlet with a Bypass Discharging from the Top or Bottom of the Diffuser in an Axial Direction. NACA RM E53A29, 1953.

3. Simon, Paul C.: Performance Characteristics at Mach Numbers to 2.0 of Various Types of Side Inlets Mounted on Fuselage of Proposed Supersonic Airplane. IV - Rectangular-Cowl Inlets with Two-Dimensional Compression Ramps. NACA RM E52H29, 1952.

4. Bailey, Neil P.: The Thermodynamics of Air at High Velocities. Jour. Aero. Sci., vol. 11, no. 3, July 1944, pp. 227-238.

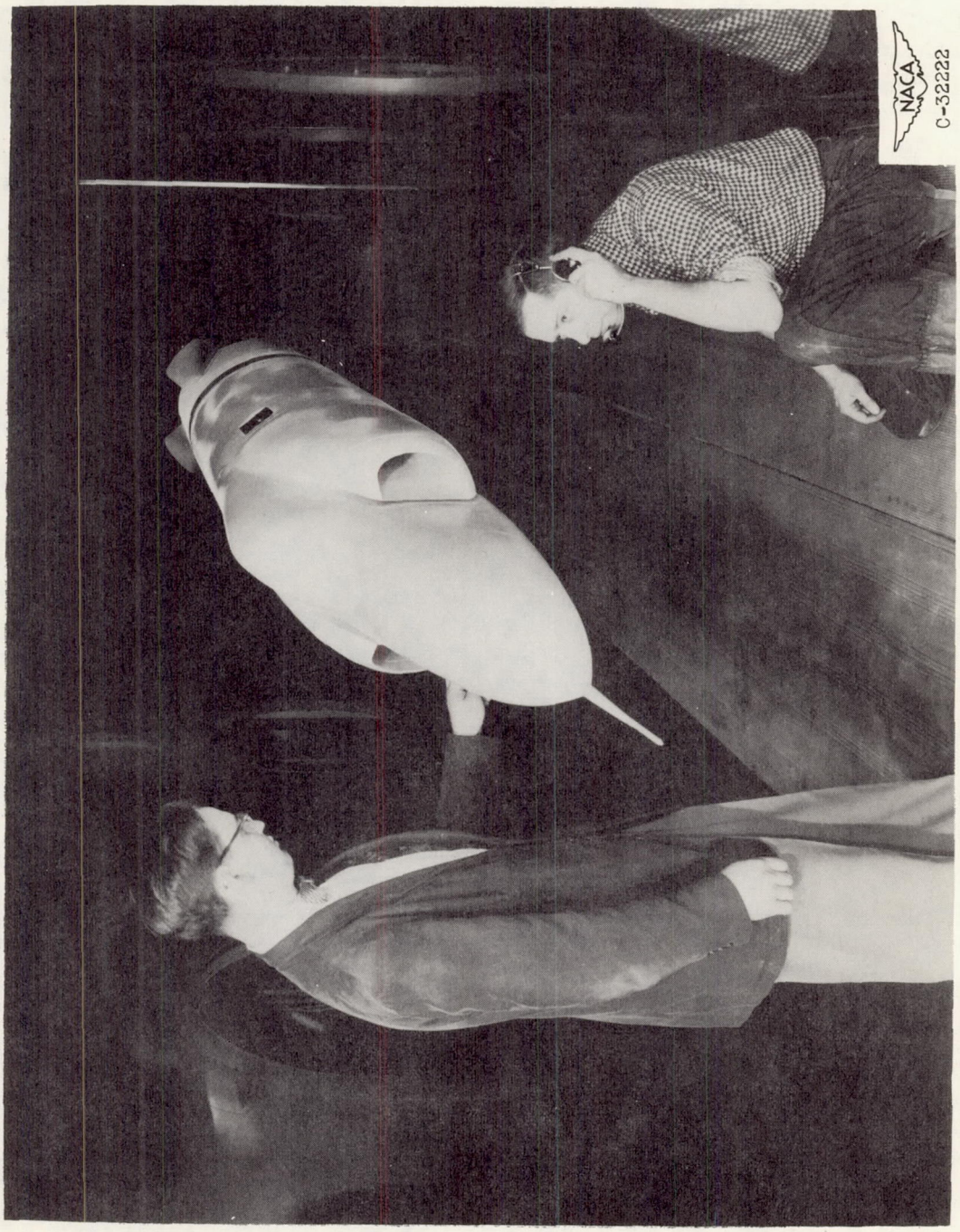

Figure 1. - Photograph of model in tunnel.

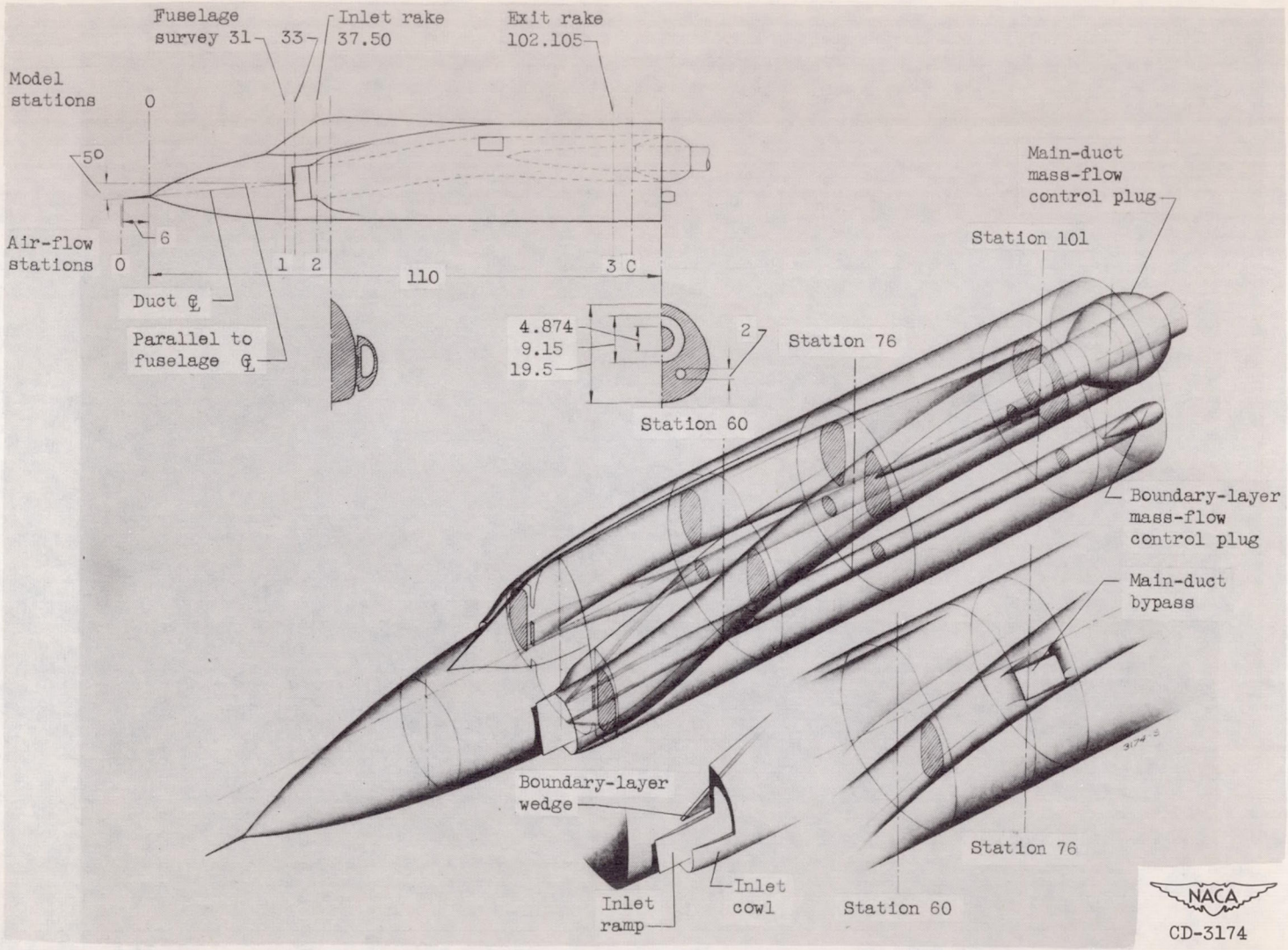

Figure 2. - Diagram of model with representative cross sections (all dimensions in inches).

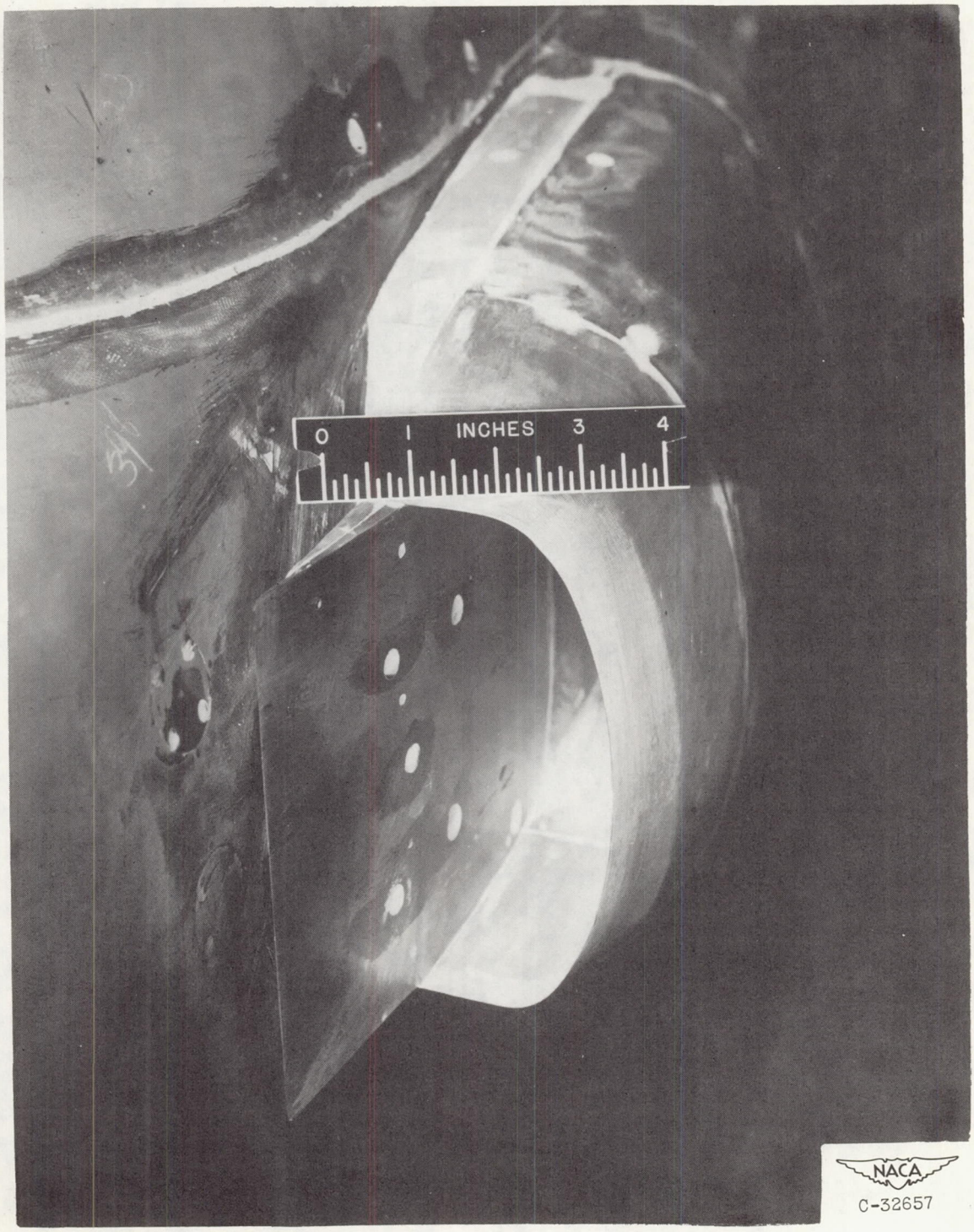

Figure 3. - Photograph of 9° ramp inlet.

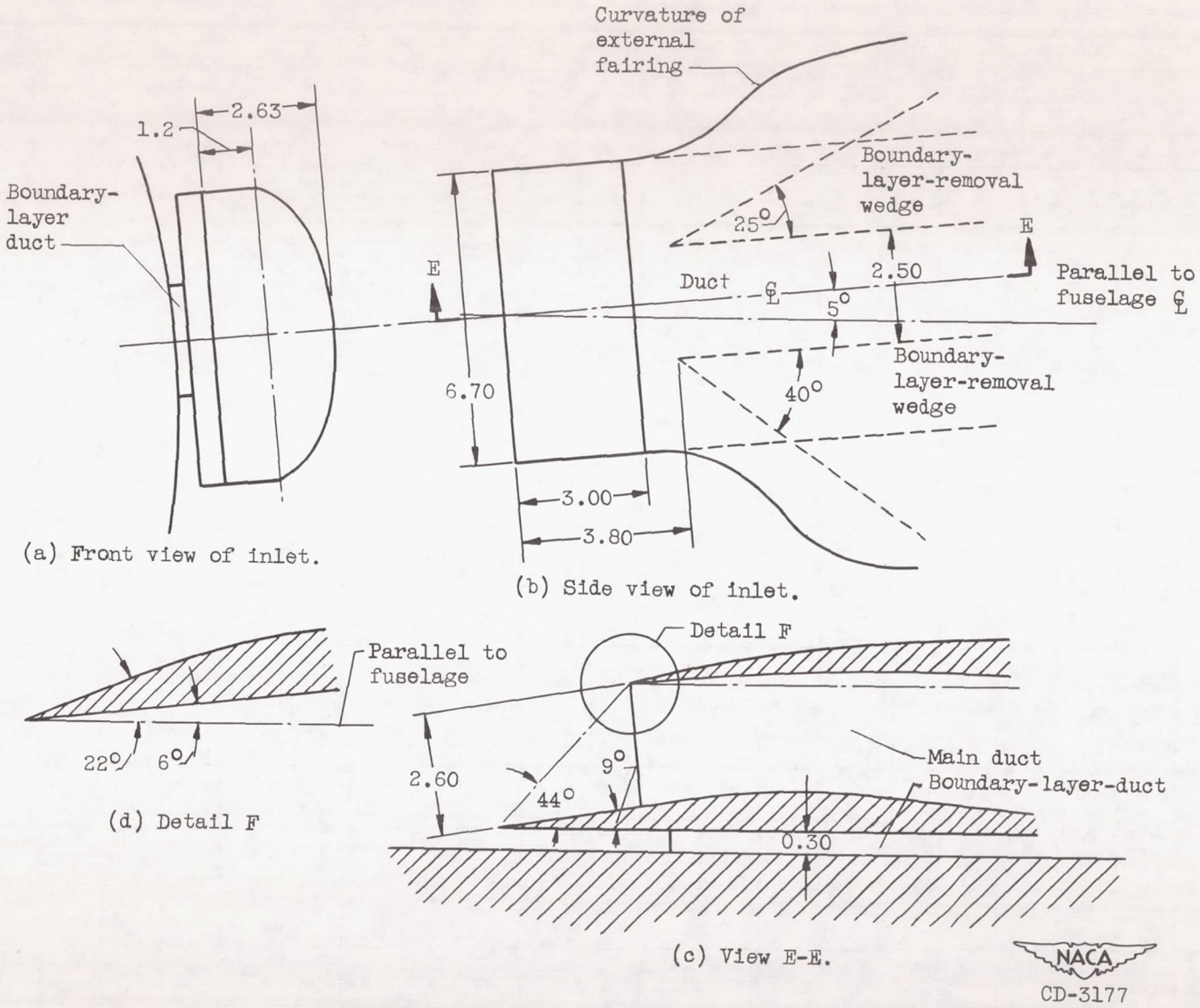

Figure 4. - Detailed views of inlet configuration (all dimensions in inches).

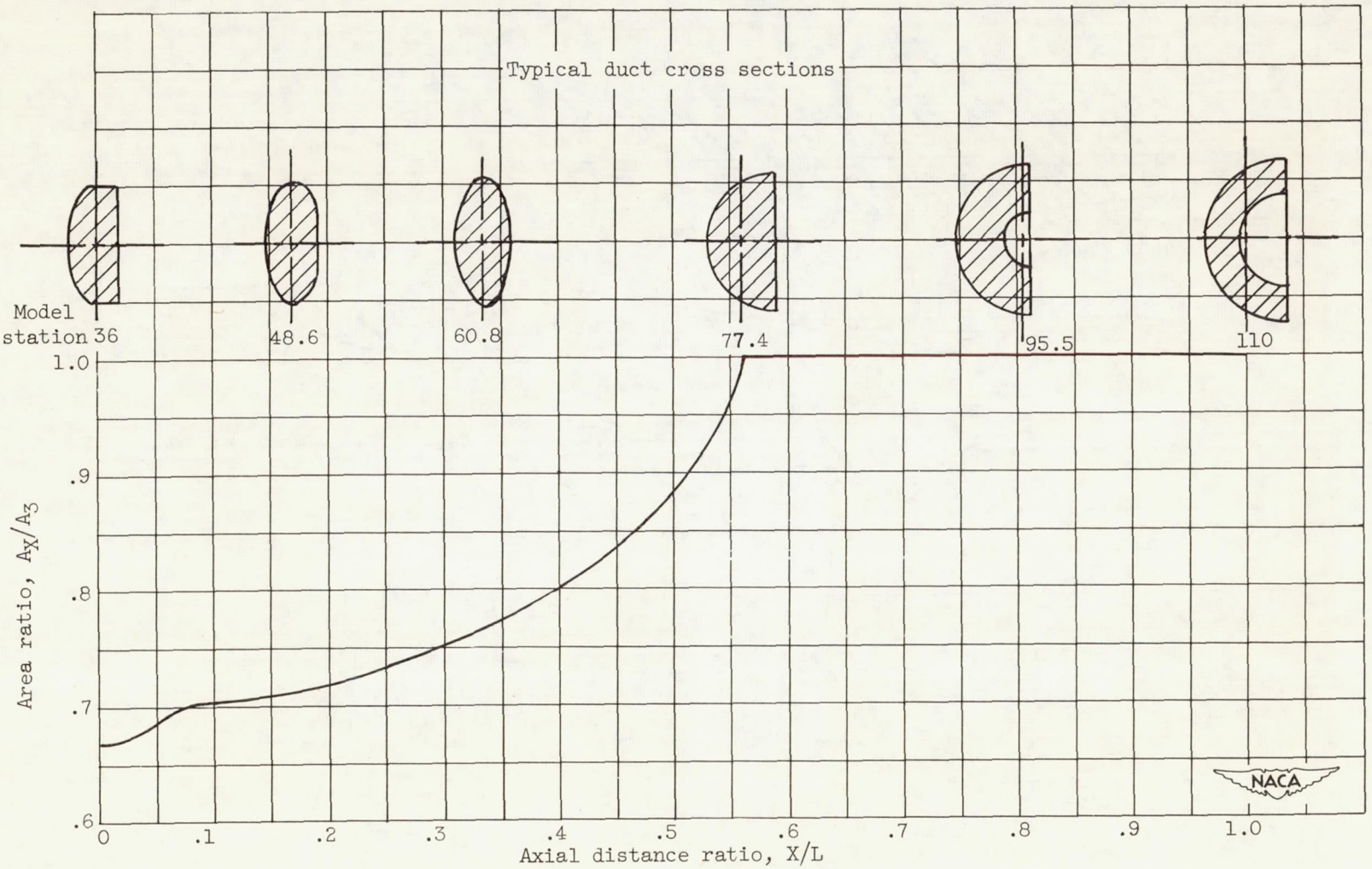

Figure 5. - Subsonic diffuser area variation.

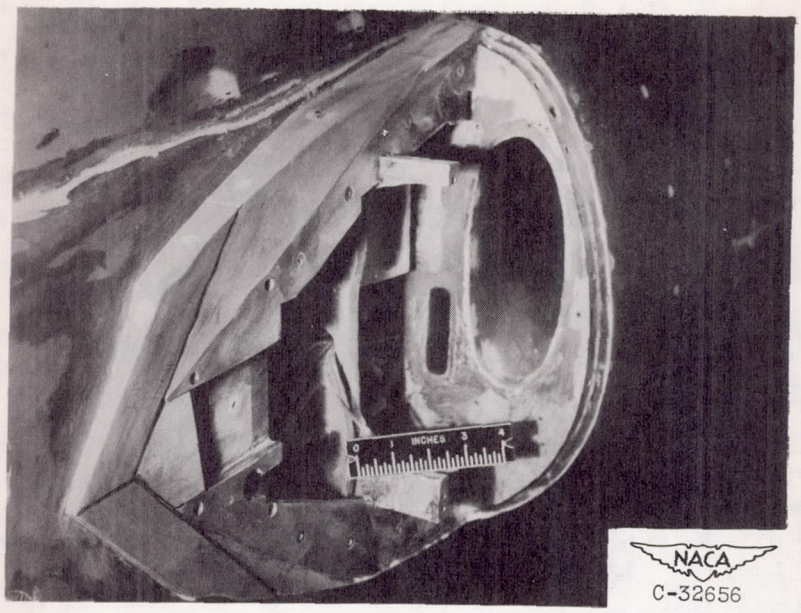

(a) Boundary-layer duct closed.

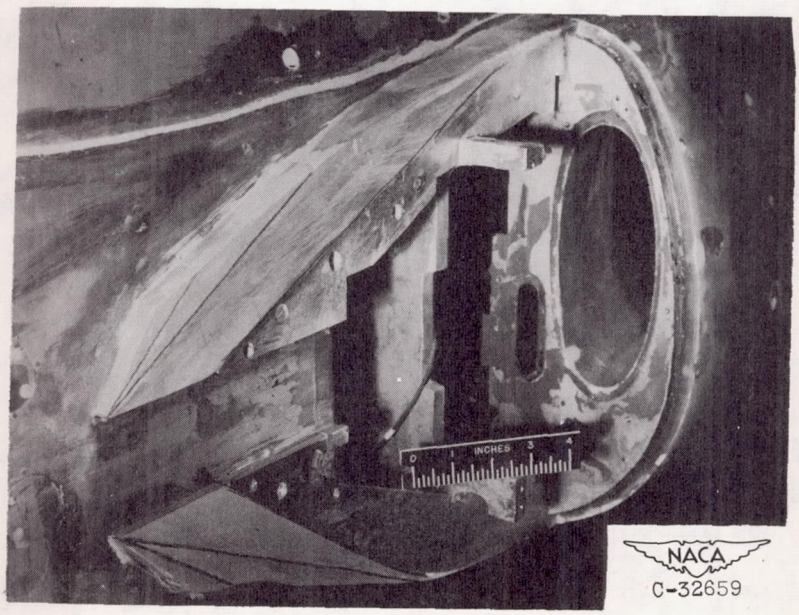

(b) Boundary-layer duct open.

Figure 6. - Photographs of various boundary-layer-removal wedge configurations.

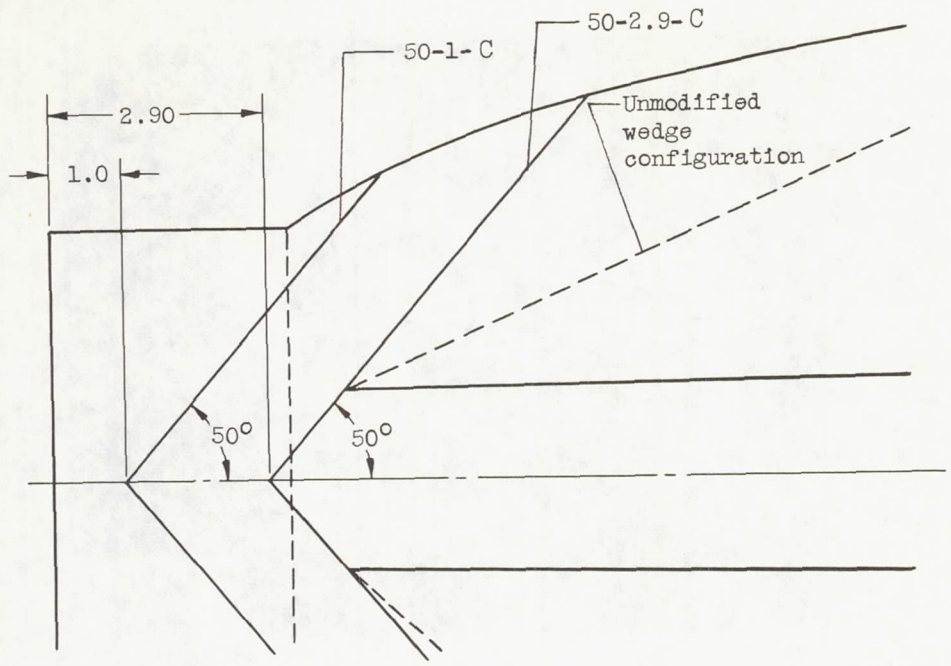

(a) Boundary-layer duct closed.

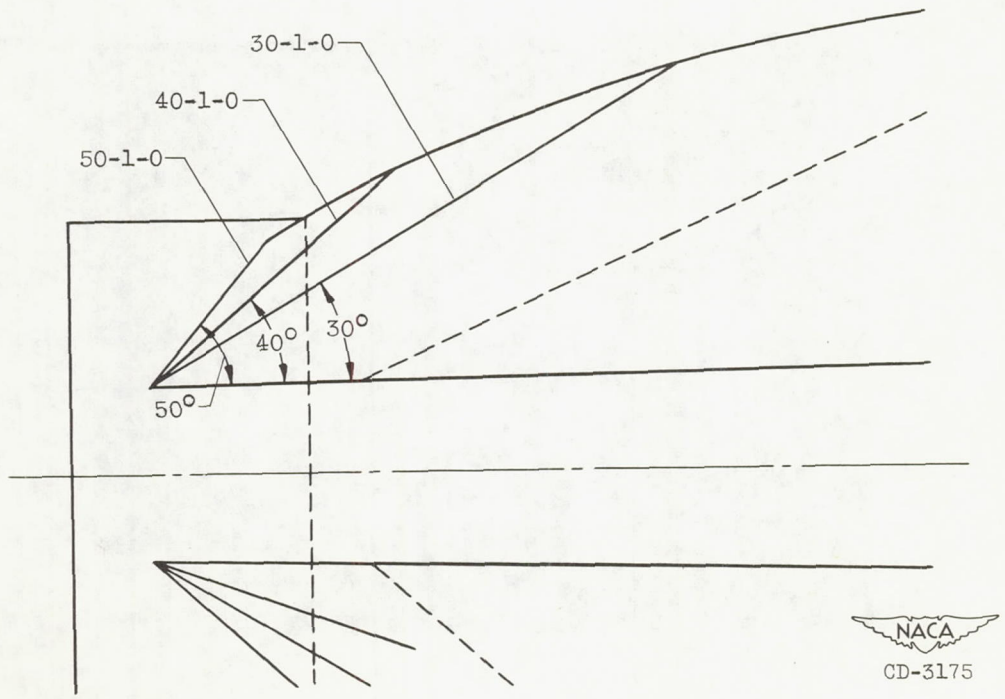

(b) Boundary-layer duct open.

Figure 7. - Boundary-layer removal wedge configurations (all dimensions in inches).

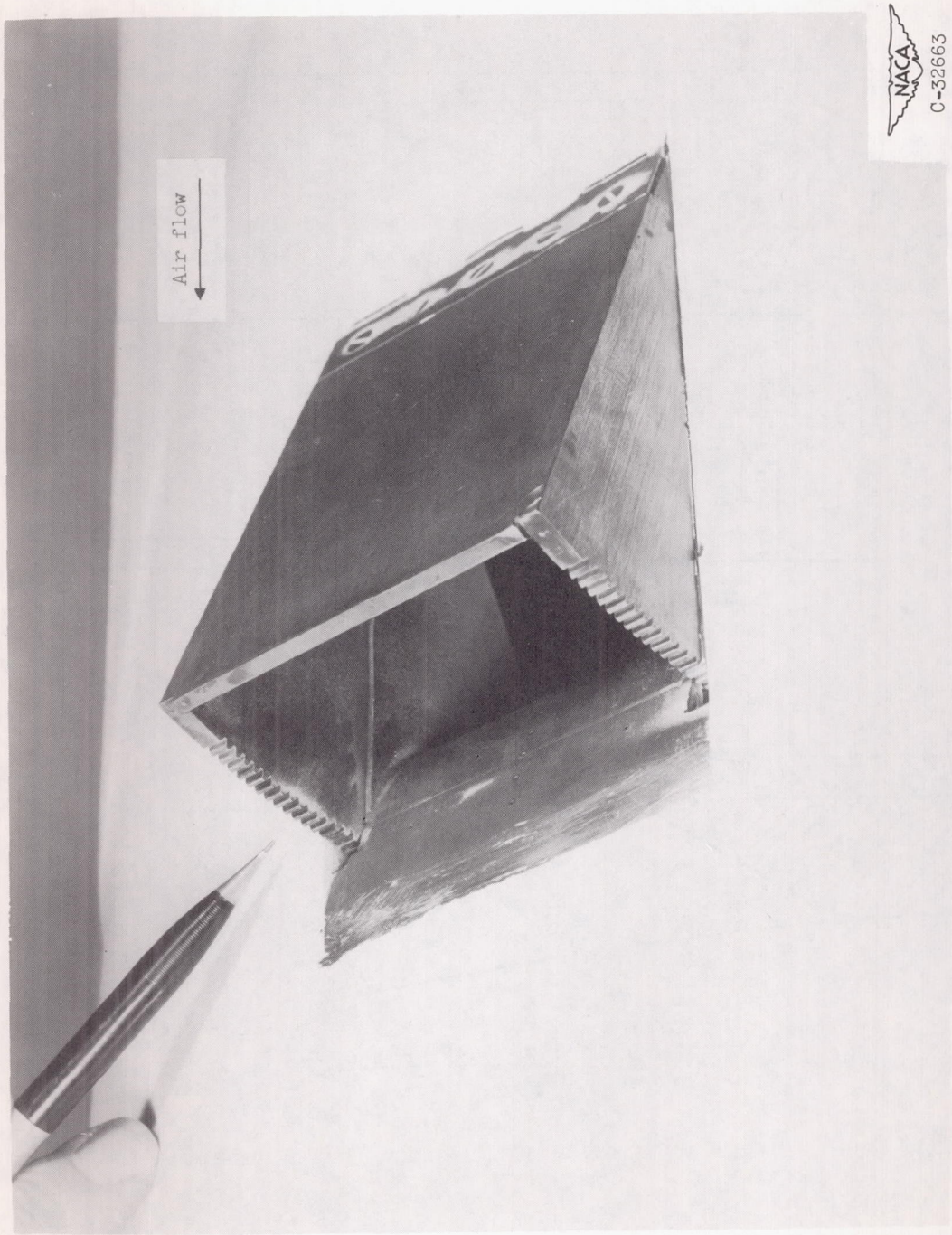

Figure 8. - Photograph of bypass system for one duct.

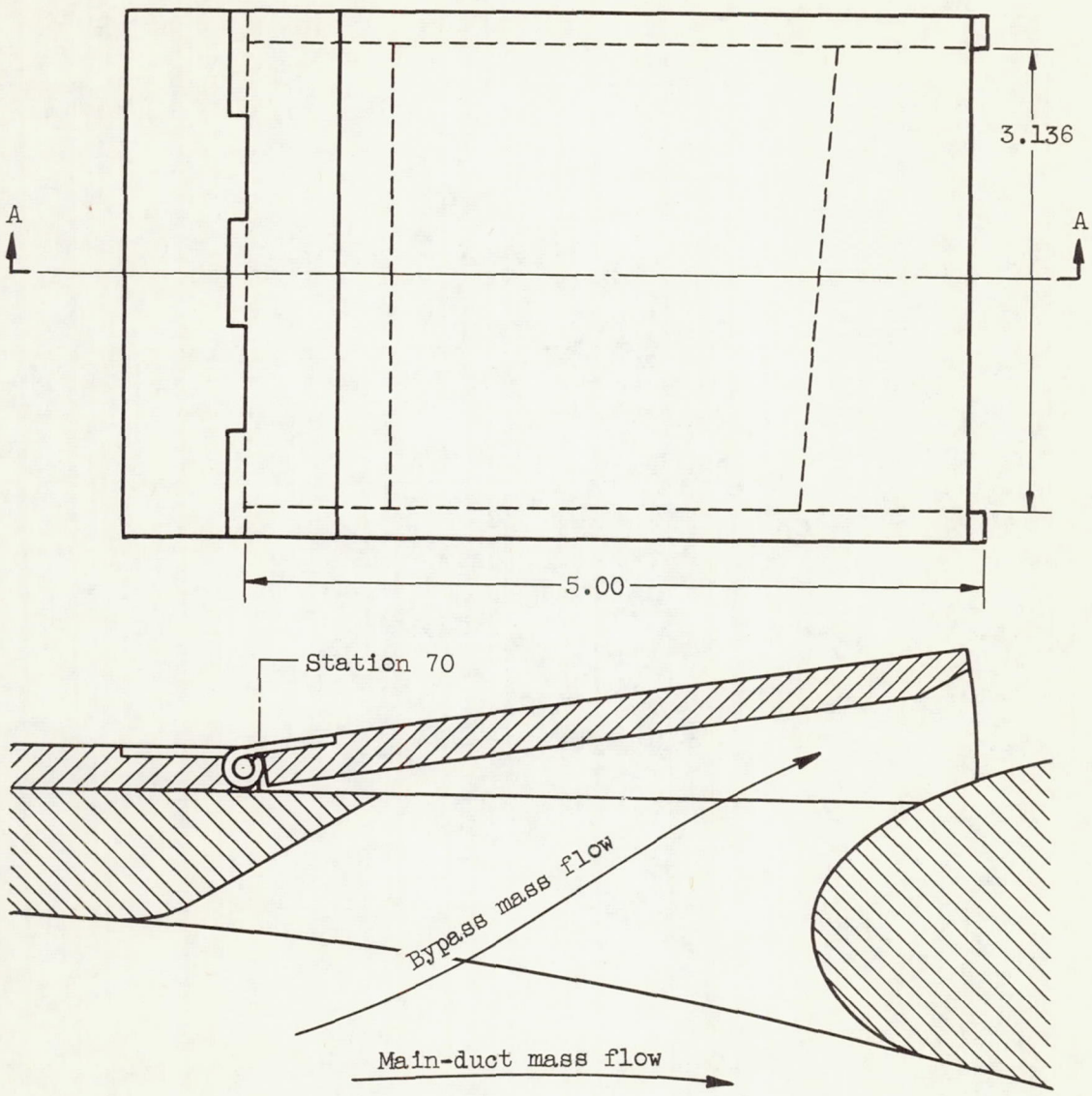

Figure 9. - Details of bypass configuration (all dimensions in inches).

CD-3176

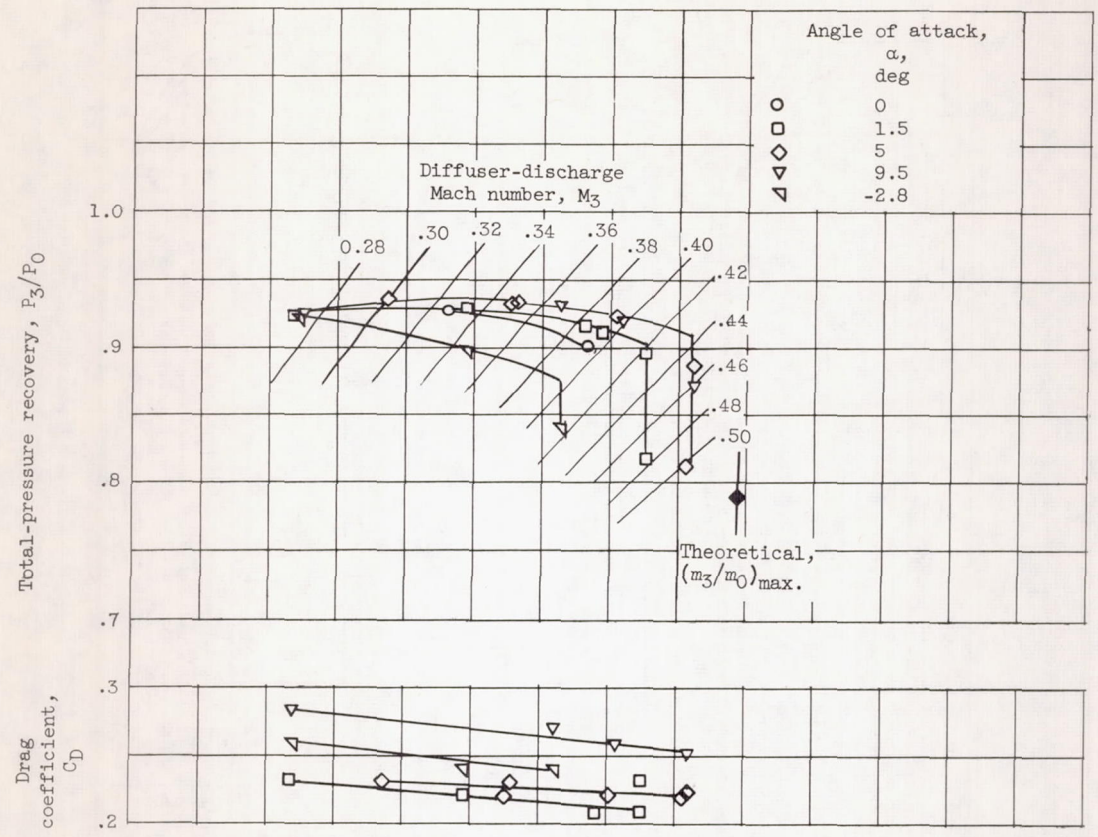

(a) Free-stream Mach number, M_0, 1.5.

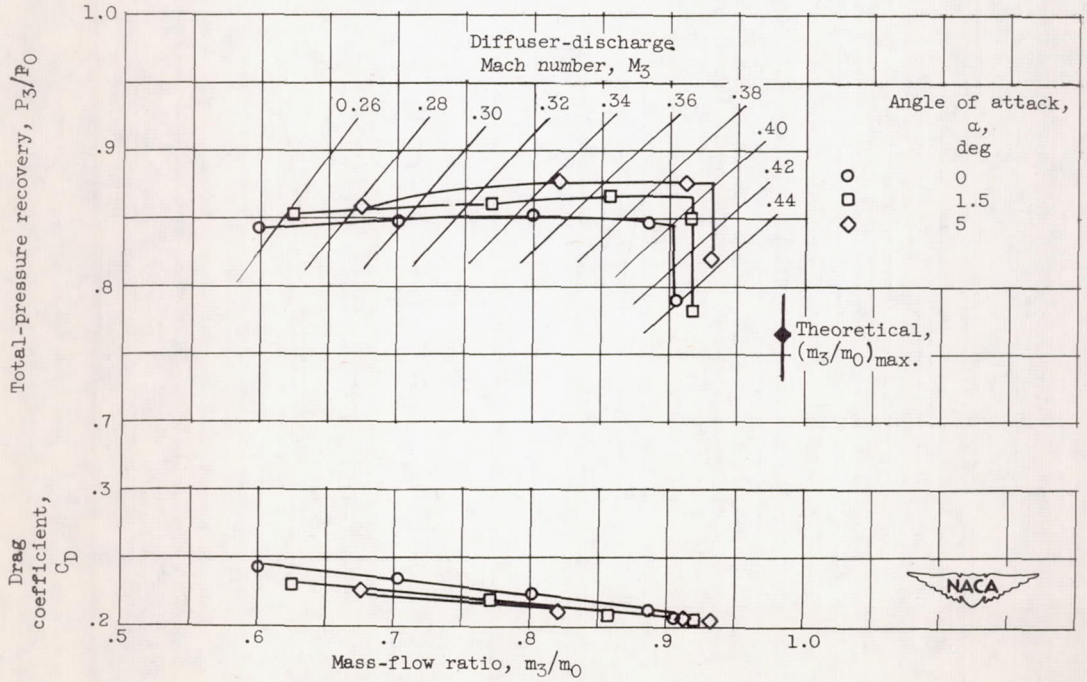

(b) Free-stream Mach number, M_0, 1.7.

Figure 10. - Performance characteristics of unmodified configuration.

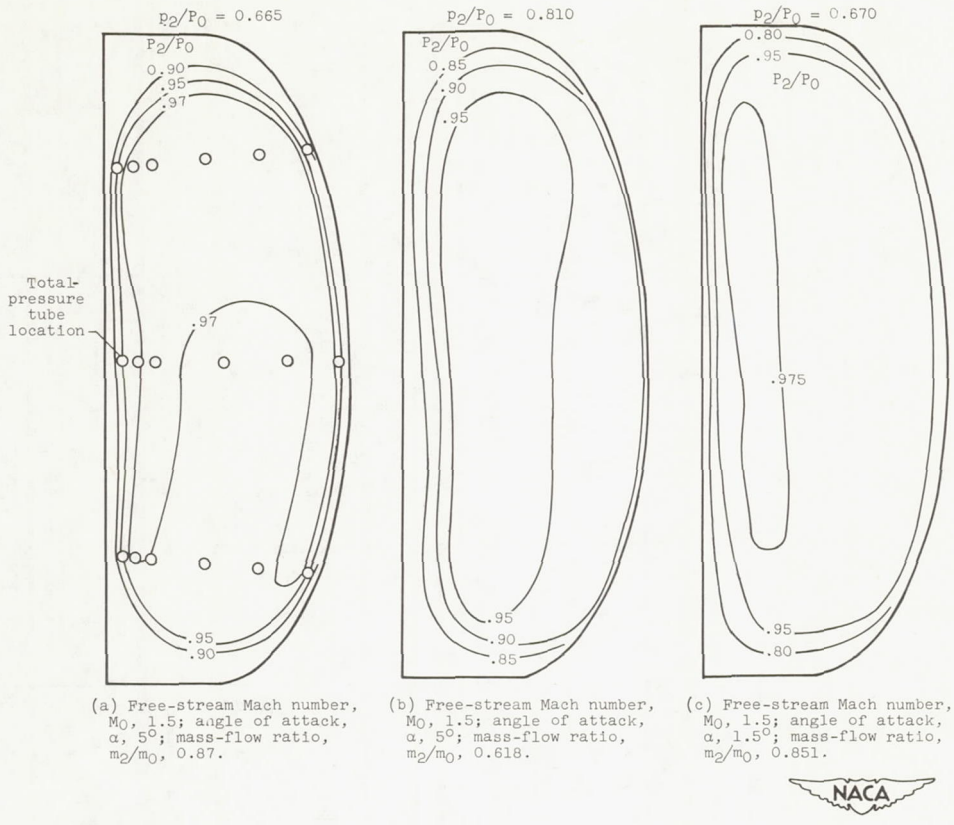

(a) Free-stream Mach number, M_0, 1.5; angle of attack, α, 5°; mass-flow ratio, m_2/m_0, 0.87.

(b) Free-stream Mach number, M_0, 1.5; angle of attack, α, 5°; mass-flow ratio, m_2/m_0, 0.618.

(c) Free-stream Mach number, M_0, 1.5; angle of attack, α, 1.5°; mass-flow ratio, m_2/m_0, 0.851.

(d) Free-stream Mach number, M_0, 1.7; angle of attack, α, 5°; mass-flow ratio, m_2/m_0, 0.821.

(e) Free-stream Mach number, M_0, 1.7; angle of attack, α, 5°; mass-flow ratio, m_2/m_0, 0.675.

(f) Free-stream Mach number, M_0, 1.7; angle of attack, α, 1.5°; mass-flow ratio, m_2/m_0, 0.785.

Figure 11. - Contours of inlet total-pressure recovery P_2/P_0 of unmodified configuration.

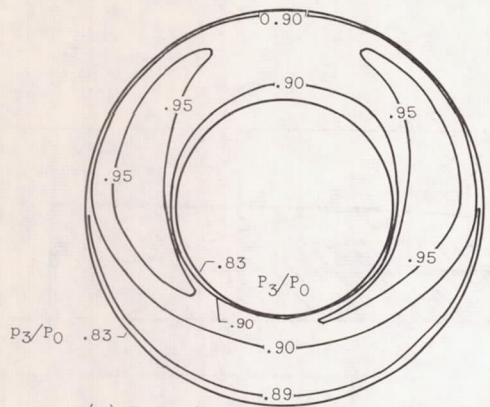

(a) Free-stream Mach number, M_0, 1.5; angle of attack, α, 5°; mass-flow ratio, m_3/m_0, 0.909.

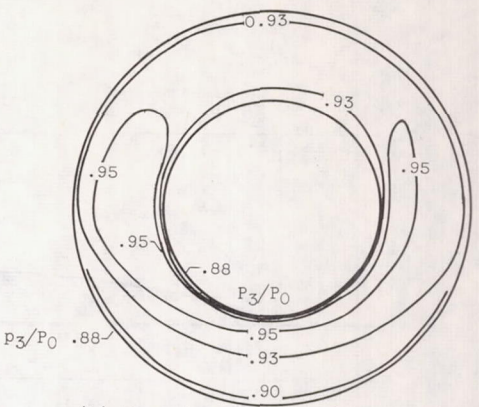

(b) Free-stream Mach number, M_0, 1:5; angle of attack, α, 5°; mass-flow ratio, m_3/m_0, 0.684.

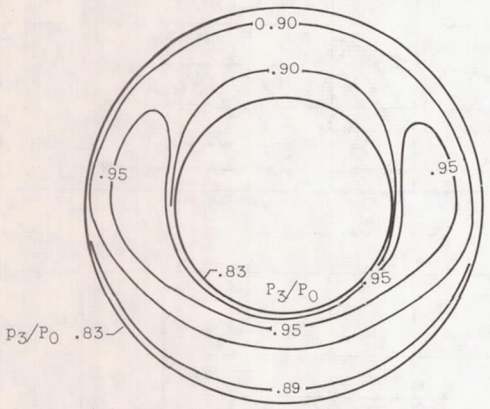

(c) Free-stream Mach number, M_0, 1.5; angle of attack, α, 1.5°; mass-flow ratio, m_3/m_0, 0.830.

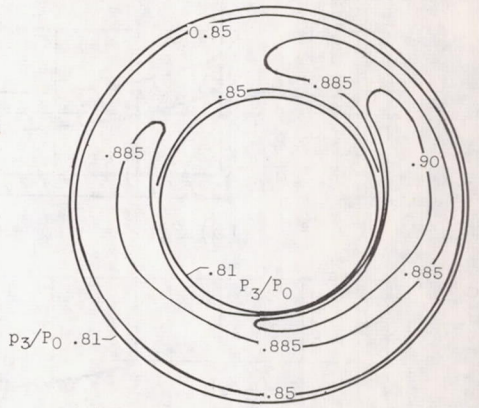

(d) Free-stream Mach number, M_0, 1.7; angle of attack, α, 5°; mass-flow ratio, m_3/m_0, 0.820.

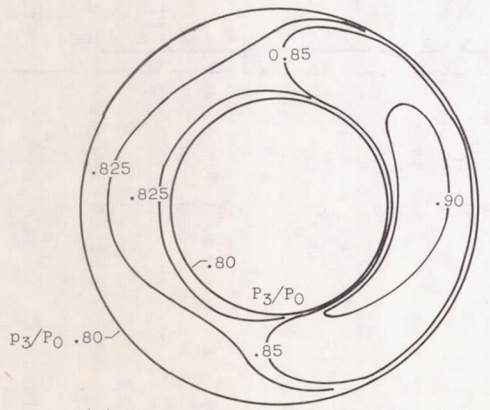

(e) Free-stream Mach number, M_0, 1.7; angle of attack, α, 5°; mass-flow ratio, m_3/m_0. 0.675.

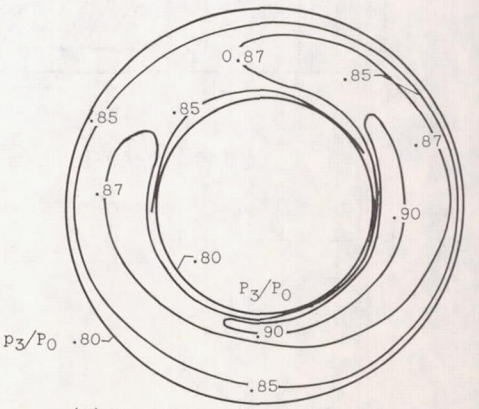

(f) Free-stream Mach number, M_0, 1.7; angle of attack, α, 1.5°; mass-flow ratio, m_3/m_0, 0.771.

Figure 12. - Contours of diffuser-exit total-pressure recovery, P_3/P_0.

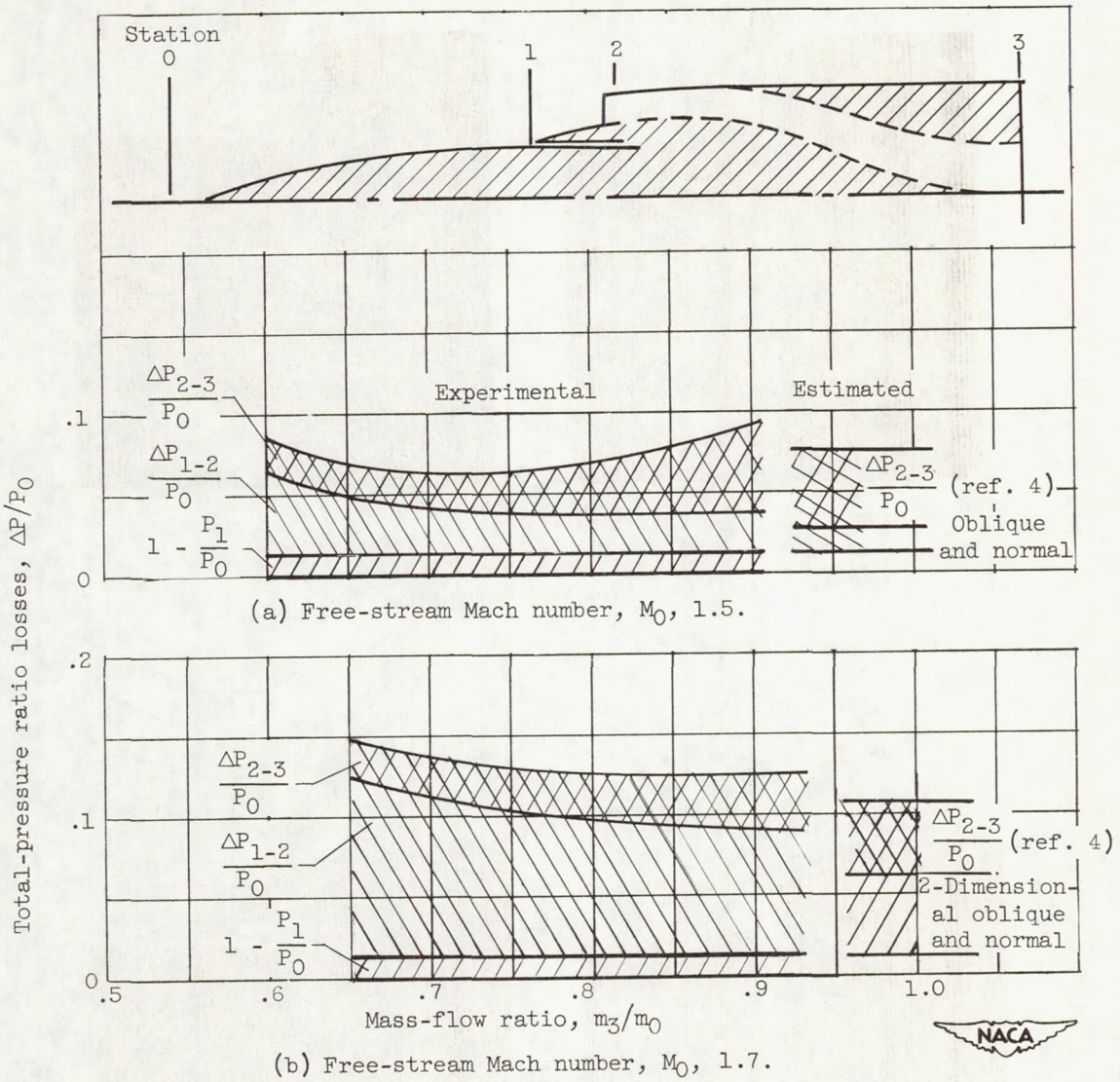

(a) Free-stream Mach number, M_0, 1.5.

(b) Free-stream Mach number, M_0, 1.7.

Figure 13. - Breakdown of total-pressure ratio losses at an angle of attack of 5°.

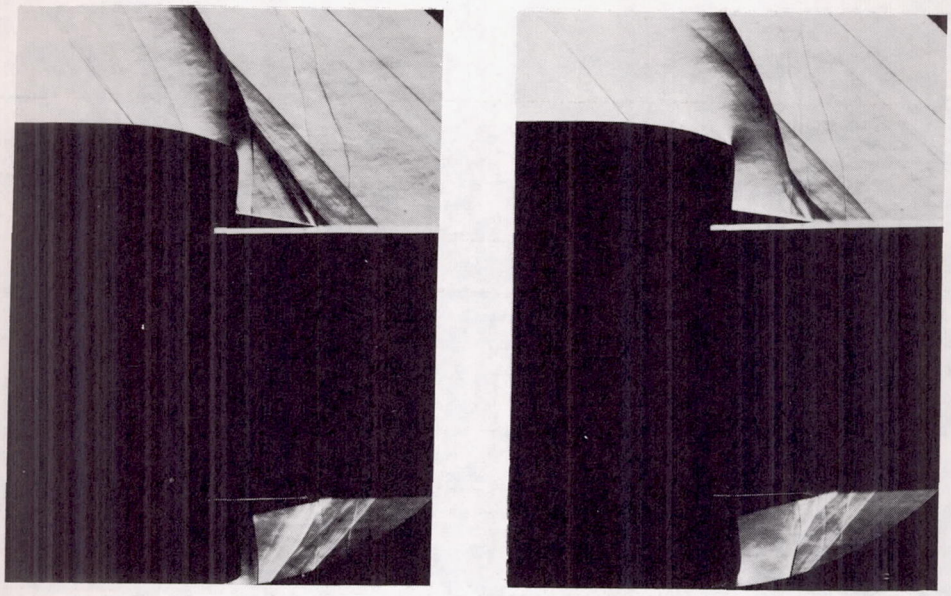

m_3/m_0 = 0.851 m_3/m_0 = 0.603

(a) Free-stream Mach number, M_0, 1.5.

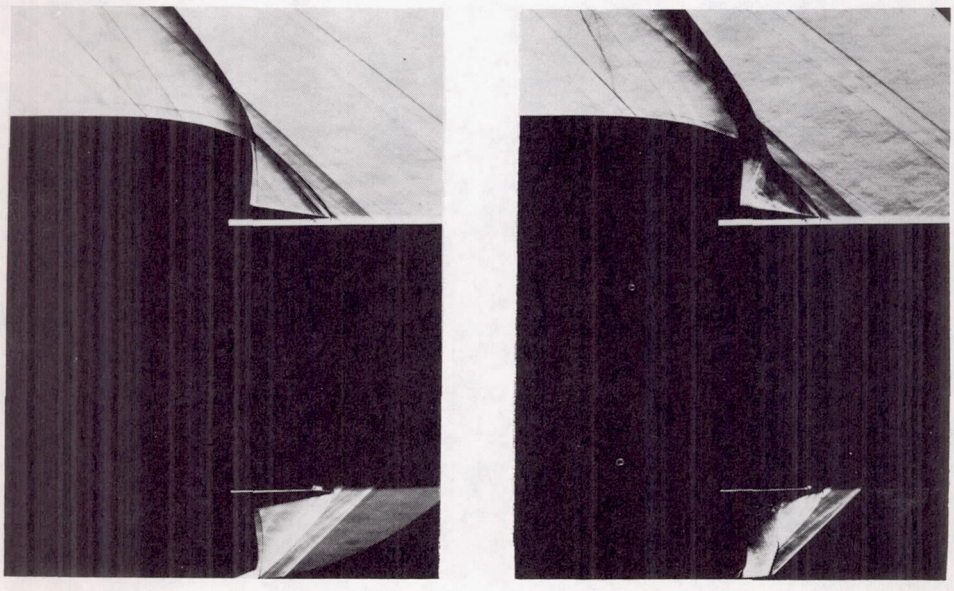

m_3/m_0 = 0.893 m_3/m_0 = 0.692

(b) Free-stream Mach number, M_0, 1.7.

C-33324

Figure 14.- Schlieren photographs of inlet at zero angle of yaw.

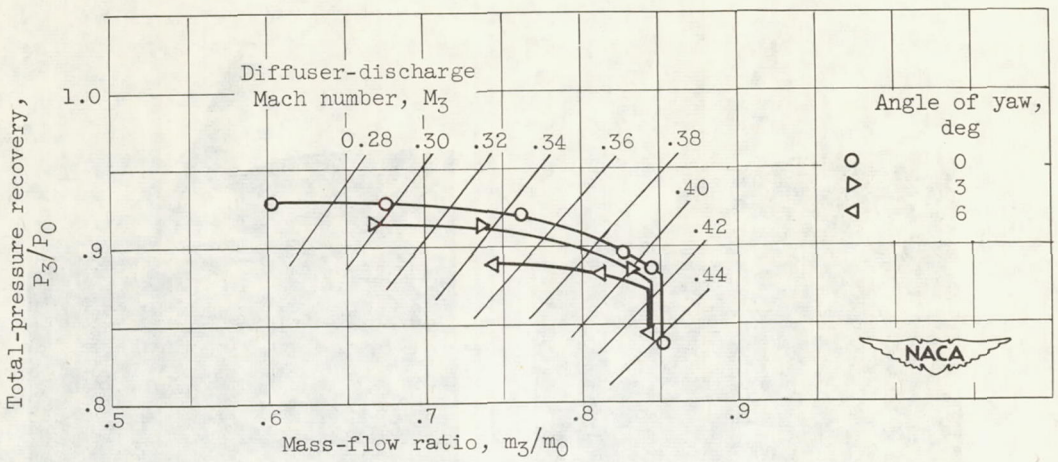

Figure 15. - Internal performance of unmodified configuration at free-stream Mach number of 1.5.

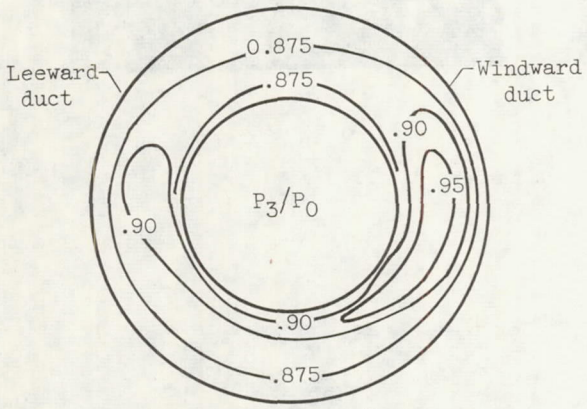

(a) Angle of yaw, 3°; mass-flow ratio, m_3/m_0, 0.833.

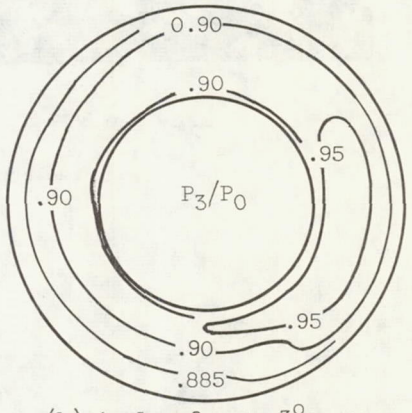

(b) Angle of yaw, 3°; mass-flow ratio, m_3/m_0, 0.738.

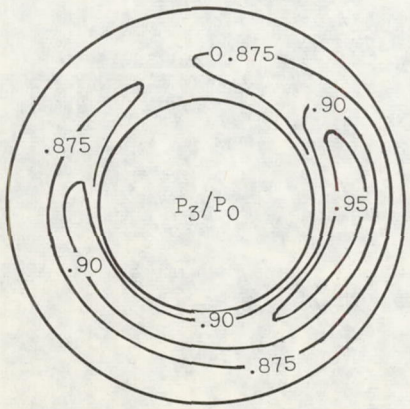

(c) Angle of yaw, 6°; mass-flow ratio, m_3/m_0, 0.814.

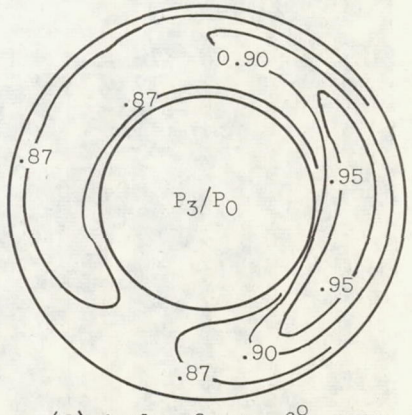

(d) Angle of yaw, 6°; mass-flow ratio, m_3/m_0, 0.731.

Figure 16. - Contours of diffuser-exit total-pressure recovery P_3/P_0 at free-stream Mach number of 1.5.

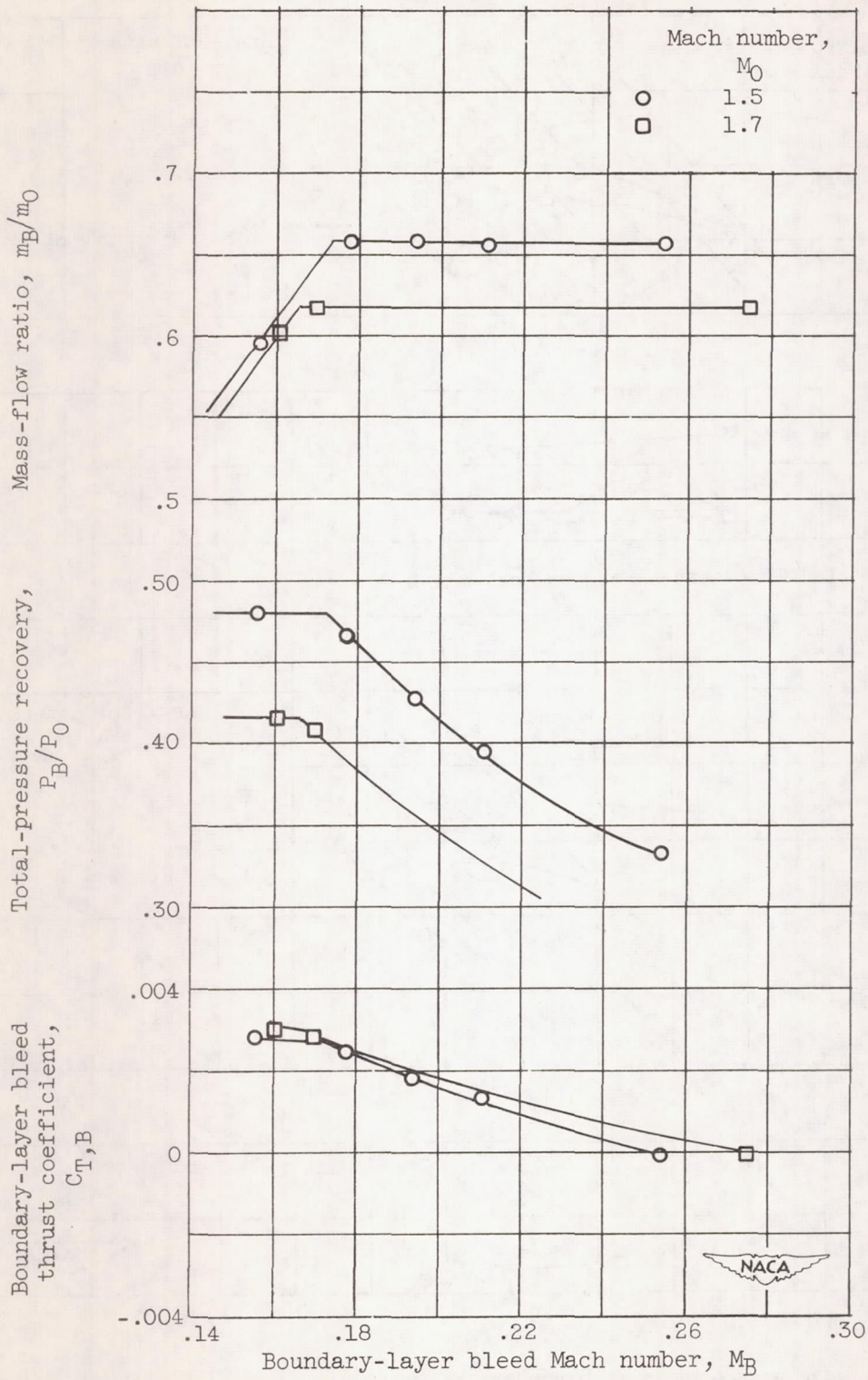

Figure 17. - Boundary-layer bleed duct performance at angle of attack of 5°.

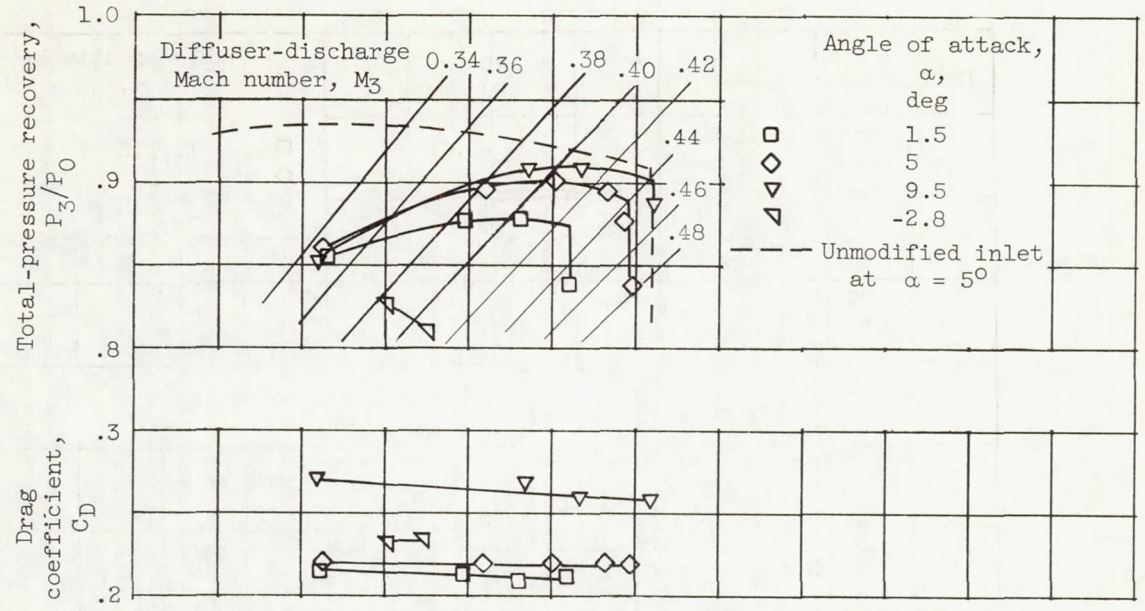

(a) Free-stream Mach number, M_0, 1.5.

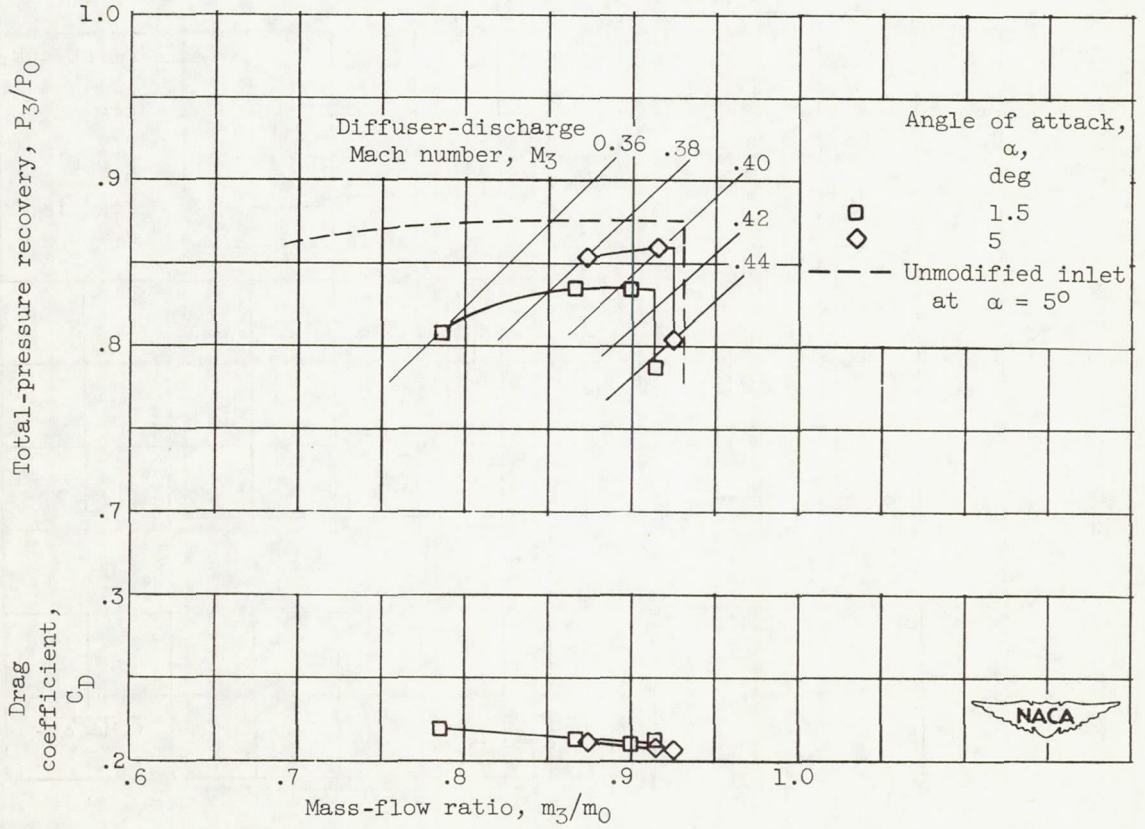

(b) Free-stream Mach number, M_0, 1.7.

Figure 18. - Performance characteristics of configuration with 50-1-C boundary-layer wedges.

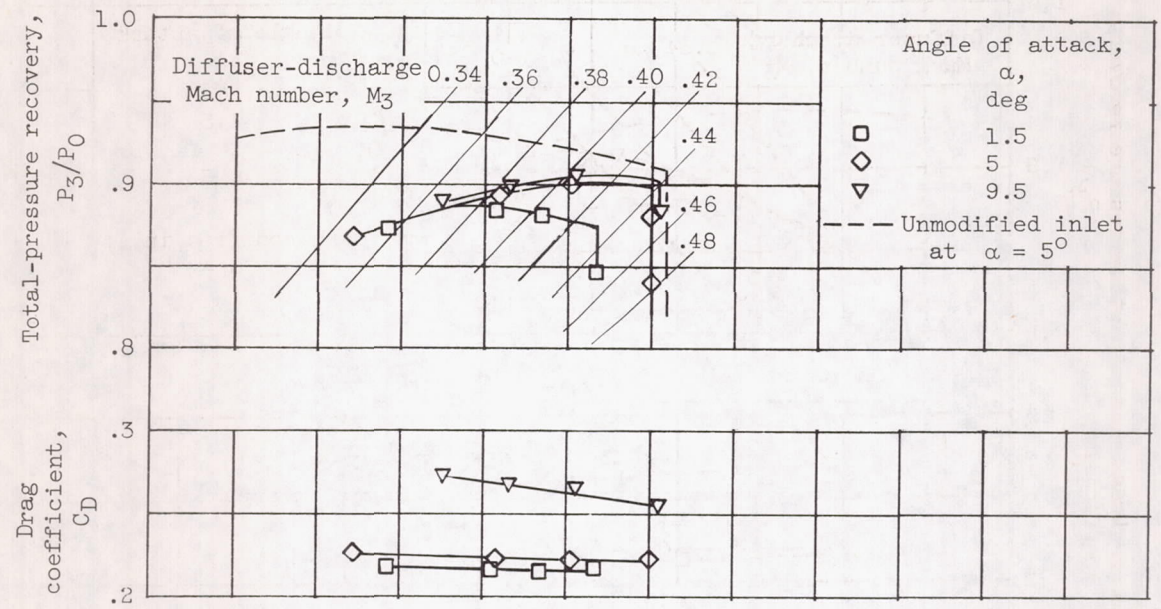

(a) Free-stream Mach number, M_0, 1.5.

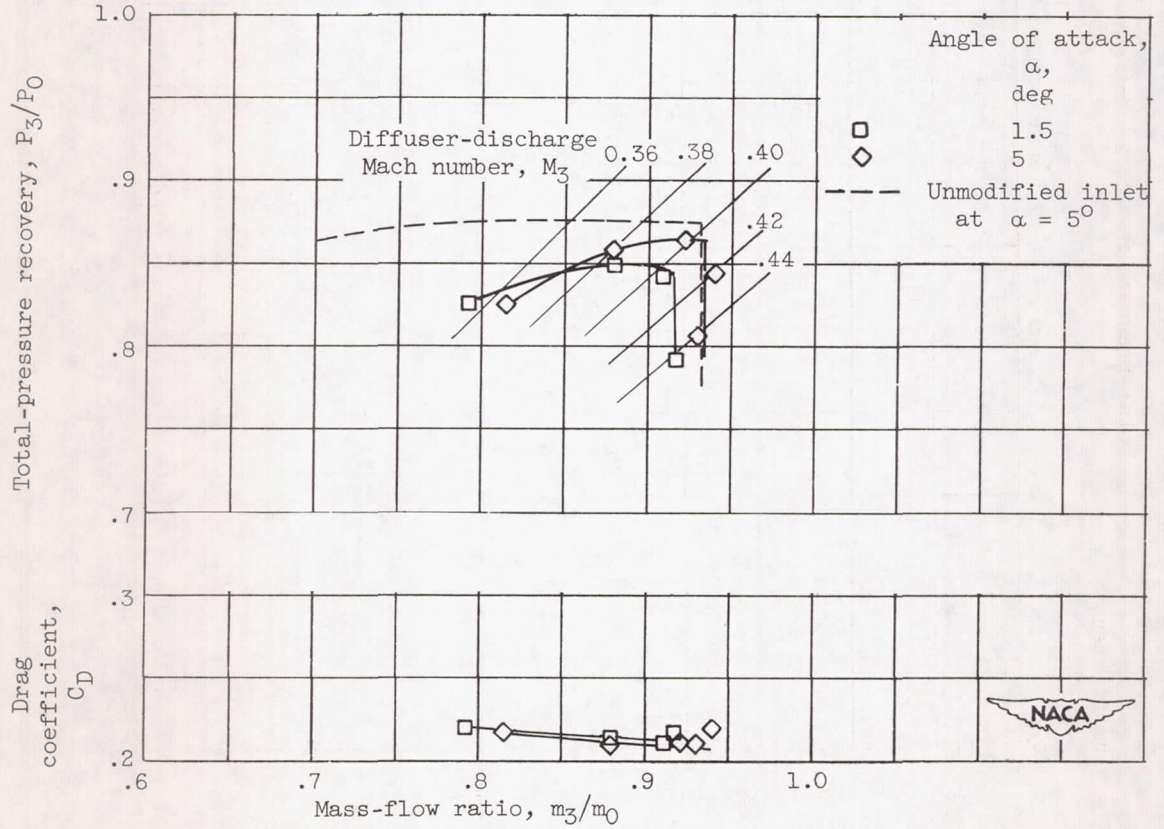

(b) Free-stream Mach number, M_0, 1.7.

Figure 19. - Performance characteristics of configuration with 50-2.9-C boundary-layer wedges.

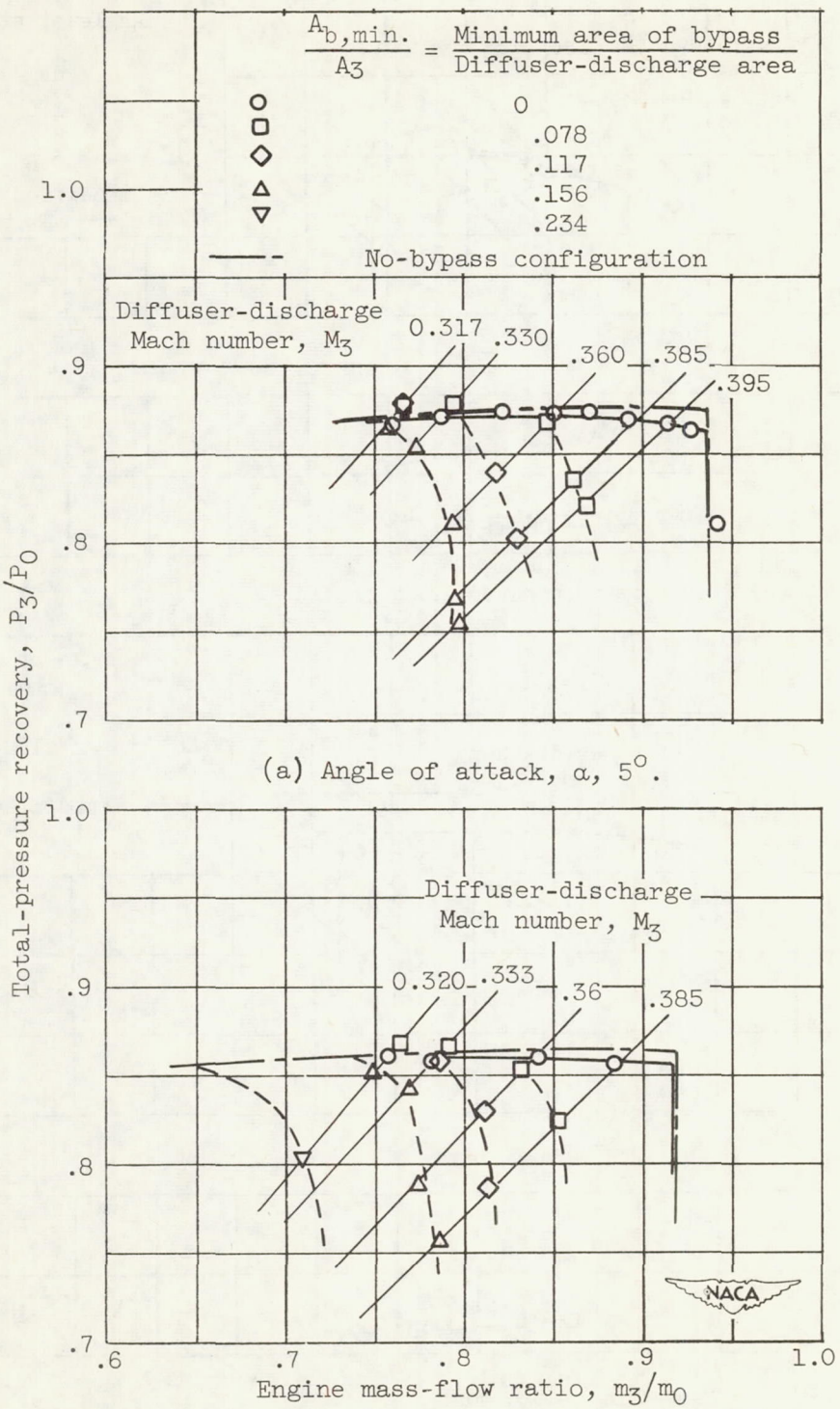

(a) Angle of attack, α, 5°.

(b) Angle of attack, α, 1.5°.

Figure 20. - Internal performance characteristics of bypass configuration at Mach number of 1.7.

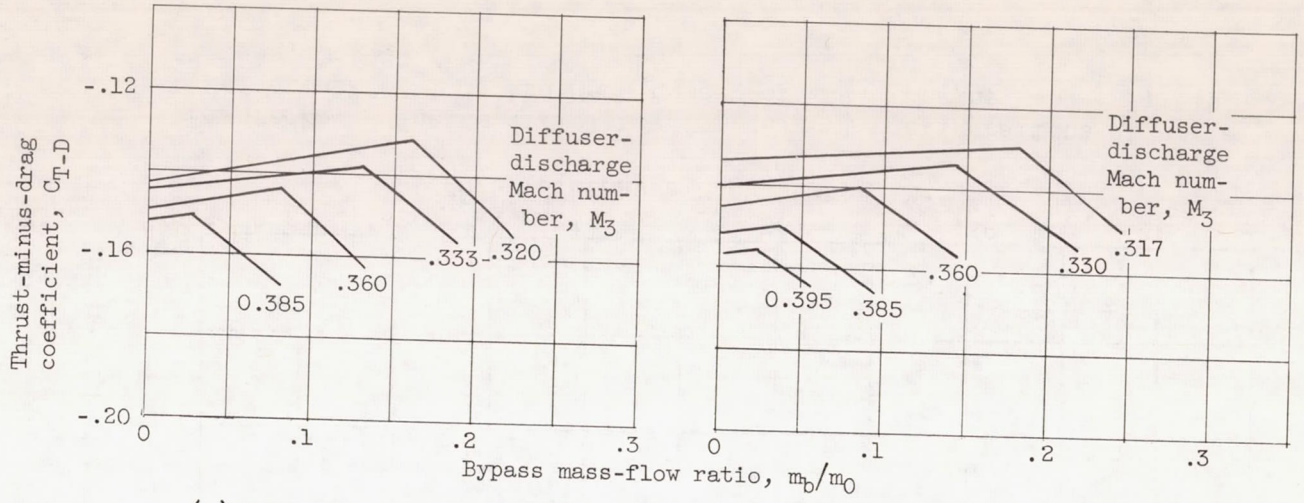

(a) Angle of attack, α, 1.5°.

(b) Angle of attack, α, 5°.

Figure 21. - Thrust-minus-drag characteristics of bypass configuration at Mach number of 1.7.

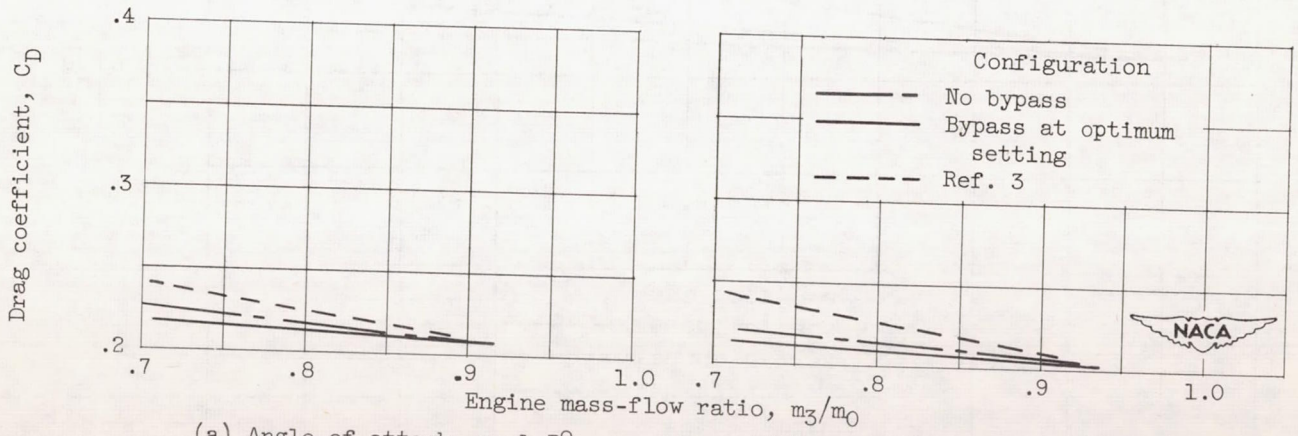

(a) Angle of attack, α, 1.5°.

(b) Angle of attack, α, 5°.

Figure 22. - Drag characteristics of several configurations at Mach number of 1.7.

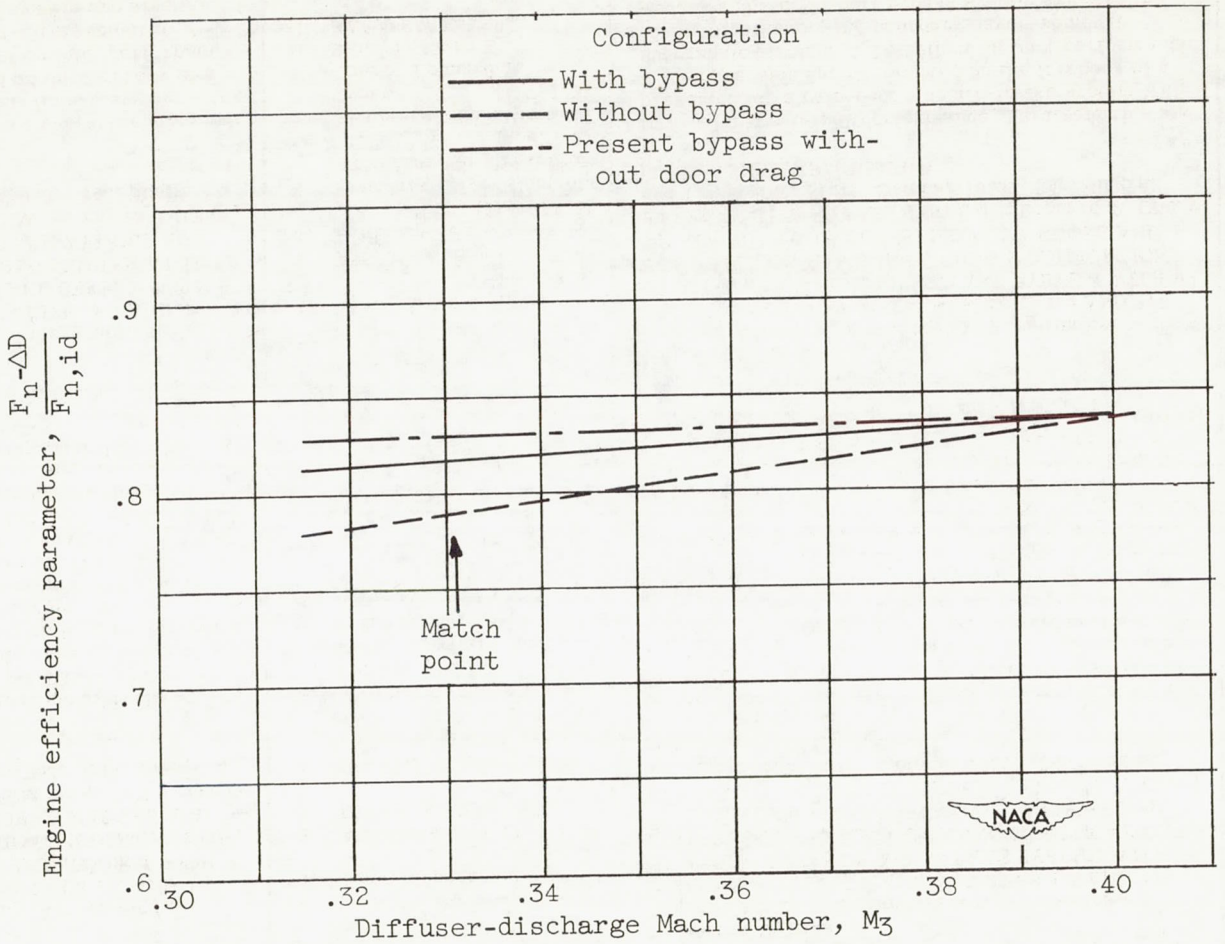

Figure 23. - Engine efficiency for several configurations at angle of attack of 1.5° and Mach number of 1.7. Engine, J57-P-7; altitude, 35,000 feet.